

Review

Safety Aspects of Sodium-Ion Batteries: Prospective Analysis from First Generation Towards More Advanced Systems

Pempa Tshering Bhutia ^{1,2,3,4} , Sylvie Grugeon ^{2,3}, Asmae El Mejdoubi ⁵, Stéphane Laruelle ^{2,3} and Guy Marlair ^{1,*} 

¹ Institut National de l'Environnement Industriel et des Risques (INERIS), Parc Technologique Alata, BP2, 60550 Verneuil-en-Halatte, France; pempa.tshering.bhutia@u-picardie.fr

² Laboratoire de Réactivité et Chimie des Solides, CNRS UMR 7314, Université de Picardie Jules Verne, 80039 Amiens, France; sylvie.grugeon@u-picardie.fr (S.G.); stephane.laruelle@u-picardie.fr (S.L.)

³ RS2E, Réseau Français sur le Stockage Electrochimique de l'Energie, FR CNRS 3459, CEDEX 1, 80039 Amiens, France

⁴ Alistore-European Research Institute (ERI), FR CNRS 3104, CEDEX 1, 80039 Amiens, France

⁵ TIAMAT, 72 Rue des Jacobins, 80000 Amiens, France; asmae.elmejdoubi@tiamat-energy.com

* Correspondence: guy.marlair@ineris.fr

Abstract: After an introductory reminder of safety concerns pertaining to early rechargeable battery technologies, this review discusses current understandings and challenges of advanced sodium-ion batteries. Sodium-ion technology is now being marketed by industrial promoters who are advocating its workable capacity, as well as its use of readily accessible and cheaper key cell components. Often claimed to be safer than lithium-ion cells, currently only limited scientifically sound safety assessments of sodium-ion cells have been performed. However, the predicted sodium-ion development roadmap reveals that significant variants of sodium-ion batteries have entered or will potentially enter the market soon. With recent experiences of lithium-ion battery failures, sodium-ion battery safety management will constitute a key aspect of successful market penetration. As such, this review discusses the safety issues of sodium-ion batteries, presenting a twofold innovative perspective: (i) in terms of comparison with the parent lithium-ion technology making use of the same working principle and similar flammable non-aqueous solvent basis, and (ii) anticipating the arrival of innovative sub-chemistries at least partially inspired from successive generations of lithium-ion cells. The authors hope that the analysis provided will assist concerned stakeholders in the quest for safe marketing of sodium-ion batteries.

Keywords: sodium-ion battery; energy storage; cell safety; cell components; full battery pack; thermal runaway



Citation: Bhutia, P.T.; Grugeon, S.; El Mejdoubi, A.; Laruelle, S.; Marlair, G. Safety Aspects of Sodium-Ion Batteries: Prospective Analysis from First Generation Towards More Advanced Systems. *Batteries* **2024**, *10*, 370. <https://doi.org/10.3390/batteries10100370>

Academic Editor: Ivana Hasa

Received: 30 July 2024

Revised: 4 October 2024

Accepted: 14 October 2024

Published: 17 October 2024



Copyright: © 2024 by the authors. Licensee MDPI, Basel, Switzerland. This article is an open access article distributed under the terms and conditions of the Creative Commons Attribution (CC BY) license (<https://creativecommons.org/licenses/by/4.0/>).

1. Introduction

Due to public awareness of limited fuel energy and greenhouse gas emissions by the internal combustion engine vehicles, researchers have started to focus on environmentally friendly alternatives and consider decarbonized electrical energy as one of the sustainable options to tackle climate change. However, its use often requires intermediate physical subsystems (thermal, mechanical, electrical, chemical, thermochemical, electrochemical, or magnetic fields) to store the produced electrical energy and release it on demand [1,2]. Hence, the concept of using rechargeable batteries was introduced to power electrical devices. In 1859, Gaston Planté invented the lead–acid battery, which showed real road, rail, and hydraulic applications, in partnership with Camille Alphonse Faure in 1881 [3]. Lead–acid batteries [4,5] include toxic lead compounds and corrosive sulfuric acid electrolytes [6]. This raises potential safety concerns when the batteries are exposed to abusive environments, and can impact environmental ecosystems. In addition, the lead production from mines causes public health concerns, affecting cardiovascular, immune, endocrine,

and reproductive systems [7]. However, owing to its cheap manufacturing, the lead–acid battery still has a dominant market share. Thereafter, Ernst Waldemar Jungner, in 1899, patented the use of alkaline electrolyte [8]. The next generation of rechargeable batteries were Ni–Cd cells, consisting of nickel hydroxides and cadmium at the positive and negative electrodes, respectively, which will be banned in the EU with all portable applications from August 2025 [9]. The havoc comes from cadmium metal instructed by the Restriction of Hazardous Substances (RoHS) EU directive 2002/95/EC, due to its carcinogenic nature, respiratory and reproductive issues, and the adverse effects it imposes on the environment [10]. Compared to Ni–Cd batteries, the enhanced Ni–MH batteries consisting of same positive electrode and intermetallic compounds at the negative electrode have 30–40% greater volumetric energy density [11] and are considerably safer and usable for consumer applications. However, the cost of production remains high due to Ni and rare earth metals in these systems, and safety precaution must be followed to prevent hydrogen leaking [12].

Following this, the initial research on advanced systems, namely Li-ion and Na-ion intercalation chemistry, started during the 1960s and the 1970s [13–15]. Advanced Li-ion batteries remain the cutting-edge technology for versatile applications, while advanced Na-ion batteries can be considered as an emerging technology to complement Li-ion batteries for large-scale energy storage applications. The first lithium-ion batteries (LiBs) commercially produced by Sony in 1991 contained lithiated cobalt oxide (LiCoO_2) as the cathode, petroleum coke as the anode [16], and aprotic organic carbonate-based solvent/lithium hexafluorophosphate (LiPF_6) salt electrolytes. They had greater energy density than pioneer rechargeable aqueous batteries, which led to the dominance of LiBs as the state-of-the-art batteries that command the portable electronic and electric vehicle markets. However, these batteries may undergo thermal runaway (TR); also a very well-known hazard in the chemical industry, battery TR is the incident when temperature of a battery cell increases due to self-heating caused by uncontrollable cascading exothermic reactions [17]. TR leads to flammable and toxic gas venting, and subsequent threats pertaining to fires and explosions events. During TR, the battery pack undergoes a series of (electro)chemical reactions: Solid Electrolyte Interphase (SEI) layer decomposition at the negative electrode, leading to electrolyte solvents reduction with intercalated lithium (sodium) ions [18], exothermic decomposition of cathode releasing oxygen (layered oxides), exothermic reaction of released oxygen with the electrolyte, electrolyte and binder decomposition, and so on [19,20]. Nevertheless, the exact order of reaction may vary depending upon cell chemistry or occur simultaneously. Different abuse conditions, namely thermal (overheating, high temperature storage), electrical (overcharging, over-discharging, higher charging rates), and mechanical abuse (physical crush, penetration) lead to TR [21]. Taking this into account, various safety measures have been developed in laboratory or large-scale tests to study the TR mechanism and the ways to curb it. Some of the methods employed are the overcharging, forced discharge test, heating test, nail penetration test, physical crush test, external short circuit test, and so on [22–24]. These tests then become the standard measures to understand TR and battery safety depending on cell chemistry, module type, and battery design.

The severity of TR depends on the chemistry of electrodes and the electrolyte materials. The most frequently used cathode families of LiBs include layered oxides as LiCoO_2 (LCO) [25–27], $\text{Li}[\text{Ni}_x\text{Co}_y\text{Al}_z]\text{O}_2$, ($x \geq 0.8$, $y = 0.1\text{--}0.15$, and $z = 0.05$) (NCA) and $\text{Li}[\text{Ni}_{1-x-y}\text{Co}_x\text{Mn}_y]\text{O}_2$ (NMC) [28–31], spinel oxides such as LiMn_2O_4 (LMO) [32,33], or olivine phosphates [34,35] such as LiFePO_4 (LFP) [36]. These materials begin to react exothermically with electrolyte in the 130–250 °C range with the thermal stability order of LFP > LMO > NMC111 > NCA > LCO. Ni-rich layered oxides are required for high-energy Li-ion battery technologies; however, their thermal stability decreases with increasing Ni content [37,38]. This instability results from the propensity of Ni^{4+} at the charge state to spontaneously reduce into Ni^{2+} [39,40]. This reduction reaction is accompanied by (i) a release of singlet oxygen (${}^1\Delta_g$ or ${}^1\text{O}_2$) reactive species that are oxidizing the electrolyte solvents [41] and (ii) phase transitions from a hexagonal to a spinel then rock-salt type phase [42]. The structure instability of Ni-rich layered material is also responsible for the gas

generation [43], and thus swelling, of the cell when stored at charge state at temperatures slightly higher than room temperature. LiFePO₄ is intrinsically considered as safer cathode material than LCO and LMO due to the inherent Fe-P-O bond, which is stronger than Co-O and Mn-O bonds; therefore, when exposed to abusive conditions, oxygen atoms are much harder to remove [44–46]. However, this statement must be taken cautiously, since field failures of LFP batteries do also occur, and from flammability and toxicity induced by TR, LFP chemistry was recently reported as more severe than NMC [47]. The selection of the ideal cathode material is still a matter of active research; however, in the quest for high performing material, the associated safety must be analyzed simultaneously. The most widely used low-potential anode materials (<0.3 V vs. Li⁺/Li⁺) in LiBs is graphite [48–50], sometimes added with silicon or silicon oxide (SiO_x) to meet high-energy LiBs requirements. The thermal runaway process is initiated by the decomposition of the SEI layer [17,51] formed from carbonate solvent and additives reduction (<1.2 V vs. Li⁺/Li⁺) on these materials upon first cycles. The TR onset temperature around 80–130 °C and heat release at the very beginning mostly depends upon the active material surface area, additives, and state of charge (SOC). The spinel lithium titanate, Li₄Ti₅O₁₂ (LTO), compound [52] whose lithium insertion/deinsertion potential (1.5 V vs. Li⁺/Li⁺) is higher than the electrolyte solvent reduction is also used as anode material [53] for low-energy batteries. In addition to being considered a “zero-strain” electrode material, which guarantees excellent capacity retention, improved safety gain is a promising feature. Belharouak et al. [54] investigated the comparative thermal behavior of charged LTO vs. graphite anodes paired with LiMn₂O₄ cathode full cells. Graphite showed an initial exothermic peak at 100 °C, whereas for LTO it was around 130 °C; moreover, the total energy released for the latter was found out to be less than the graphite anode.

Despite the dominance of LiBs, sodium-ion batteries (SiBs) are emerging as promising next-generation alternatives to complement the growing energy demand because sodium is widely available, much cheaper, and exhibits similar chemistry to that of lithium. They are considered as the best candidate power sources, even if they might lack in terms of specific energy due to the higher standard redox potential of Na⁰/Na⁺ (−2.71 V vs. SHE) vs. Li⁰/Li⁺ (−3.04 V vs. SHE) and the heavier atomic weight of Na (22.9 g·mol^{−1}) vs. Li (6.9 g·mol^{−1}). The specific capacities of selected lithium and sodium active materials are presented and compared in Table 1. Lithium-ion batteries have gravimetric energy densities ranging from 120–285 Wh/kg and volumetric energy densities between 325–785 Wh/L, depending on the specifications of cell chemistry [55]. On the other hand, sodium-ion batteries have lower gravimetric energy densities, so far announced between 100–160 Wh/kg at the cell level [56,57]. As per Table 2, sodium-ion batteries based on HC negative active material and layered oxides or Prussian white analogues, as positive active material feature maximum gravimetric energy densities of 160 Wh/kg at the cell level. Conversely, employing Prussian blue analogues on both electrodes (Natron Energy) provides low energy density, but it can be used for high power applications. The current direction of research is to improve sodium-ion battery performance at the module level and make it at least as competitive as low energy density lithium-ion chemistries like lithium iron phosphate.

Recently, sodiated layered transition metal oxides and polyanions have been introduced as advanced cathode materials and hard carbon materials as anodes for SiBs. The first generation of SiBs, commercialized by the start-up TIAMAT Energy, utilize prismatic and cylindrical high-power batteries [58] consisting of a structurally robust polyanionic cathode material Na₃V₂(PO₄)₂F₃ (NVPF) with a screwdriver in real-life application [59]. One of the pioneer UK-based startup company, Faradion Limited, manufactures high-energy cells based on the substituted and structurally stabilized layered oxide cathode material, Na_aNi_(1-x-y-z)Mn_xMg_yTi_zO₂ [60]. This technology, developed in collaboration with Williams Advanced Engineering and Oxford University, is aimed for use in electronic bikes [61].

The sodiated layered metal oxides positive active material ($\text{Na}_{1-x}\text{MO}_2$, where M is a transition metal = Mn, Ni, Ti, Zn, Fe, Co and their mixtures) are classified into O₃ and P₂ type materials [62]. These are based on the oxide layer stacking in octahedral or prismatic environment of Na ions and the numbers 2 and 3 are the transition metal layers with different octahedral coordination stacking in a unit cell [63]. These P₂, O₃, and nanoscale mixtures of O₃-P₃- or O₃-P₂-type layered oxide materials can be used in SiBs for medium to high-energy storage applications [64]. P₂-type oxides show superior structural integrity and capacity retention, and high Na^+ conduction, compared to the O₃-type oxides due to huge occupying sites and greater diffusion pathways for Na^+ [65]. Because of the presence of oxygen in the skeleton framework, it is interesting to compare the rate and temperature at which oxygen evolution occurs and how it differs from Li-ion systems. The higher the temperature at which oxygen release from layered oxide cathode occurs, the later sharp temperature increase contributing to TR is observed. Such an increase in critical temperature leading to oxygen release can contribute to the overall safety and reliability of battery systems. Polyanionic compounds are also used as sodiated positive active materials. They contain tetrahedron anion units $(\text{XO}_4)^{n-}$ or their derivatives $(\text{X}_m\text{O}_{3m+1})^{n-}$ (X = S, P, Si, As, Mo, or W) with strong covalently bonded MO_x polyhedra (M = transition metal) [66] which improves the stability of oxygen in the structure, thus offering better thermal stability compared to that of layered oxides. Due to the rigidity of the polyanionic structure, the particles show little change in volume during insertion and extraction of Na^+ ions, which also enhances their thermal stability. Hence, such active materials must be promoted due to their safety gain, and finding ways to increase their energy density must be explored [67–69]. Other materials such as Prussian blue have also been introduced as cathode materials for SiBs by Natron Energy Technology [70,71]. Prussian blue and its analogues possess the general formula $\text{Na}_x\text{M}_1[\text{M}_2(\text{CN})_6]_y \cdot n\text{H}_2\text{O}$, where M₁ and M₂ are transition metals [72]. The electrochemical performances of Prussian blue analogues (PBAs) are significantly affected by the different transition metals, the intrinsic crystalline water, and vacancies in the structure [73]. Due to its poor structural stability, it thermally decomposes to form HCN and cyanogen gas, which are equally major safety hazards [74]. Safety and environmental issues bound to potential byproducts such as HCN and NaCN indeed deserve due considerations on the full material's life cycle, as recently discussed by Xiao et al. [75]. Currently, it appears that, of the three, layered oxides and polyanionic compounds are leading the race for ideal cathode material for sodium-ion batteries, both in terms of electrochemical performance and safety.

As for anodes of SiBs, recent developments have used carbon-based materials, conversion materials, alloying compounds, and organic compounds [76]. The ion storage mechanism follows intercalation mechanism, and conversion or alloying reactions [77,78]. Carbon-based materials are the primary choice, wherein graphite has been the commercial anode material for LiBs. However, Na-graphite intercalation compounds are thermodynamically unstable and the low binding energy between sodium ions and graphite restricts its operation [79]. Non-graphitic carbons like soft carbon and hard carbon are other candidates for anode materials. The former can be converted to graphite when annealed at high temperature, while the latter does not lose its non-graphitizable behavior. However, for the practical utilization of sodium-ion batteries, low-cost hard carbon (HC) material remain the state-of-the-art anode material. It consists of randomly arranged single-layer graphite which are stacked in a random orientation. This non-graphitizable carbon type can maintain its disordered structure, in an inert atmosphere, even at a high temperature exceeding 2000 °C [80]. The carbon-based anode materials follow intercalation ion storage mechanism. Conversion-based materials undergo complete phase transition during uptake of Na^+ , involving the breaking and formation of chemical bonds [81]. Here, the complete reduction of transition metal to the metallic state occurs, offering high theoretical capacities but endures severe structural and volume changes. The type of metal present in these compounds determine its ability to undergo intercalation or alloying reactions along with conversion reactions. Sodium can form alloys with elements from group 14 and

15 including metals (Sn, Bi), metalloids (Si, Ge, As, Sb), and polyanionic nonmetal compounds (P); therefore, these materials can be used as anodes for SiBs [82]. However, most of these compounds undergo huge volumetric changes, restricting its utilization. Organic molecules offer inherent fast reaction kinetics, high energy/power density, metal-free, and environmentally friendly benefits [83]. However, the intrinsically low conductivity and easy active material dissolution in organic electrolytes limits its practical application [84]. It is worthwhile to mention that even though hard carbon remains the sole winner in the race of anode materials, it might not be the safest choice. Since the maximum capacity contribution potential of hard carbons occurs around 0–0.1 V [85], this electrochemical potential lies close to sodium metal plating potential. This can risk sodium metal deposition and cause serious safety threats. Hence, a better alternative would be to use different anodes whose redox potential is higher than sodium plating potential. In SiBs, the redox potential of titanium-based anodes (Ti^{3+}/Ti^{4+}) lies between 0.5 V to 1.0 V, and the voltage range of soft carbon sodium storage typically ranges from 0.2 and 1.2 V [86]. The choice of these anode materials avoids sodium plating, but the higher voltage range decreases the electrochemical potential window of the overall battery. Hence, increased anode safety might come at the expense of lower energy density. Therefore, the optimum trade-off between high energy batteries and safer batteries must be well balanced to ensure security.

Some of the selected first-generation variants of sodium-ion batteries are presented in Table 2. The more advanced systems refer to cathode materials for high energy batteries focusing on sodiated layered oxides utilizing abundant transition metals like Fe and Mn. Uniform surface coating on these materials could limit moisture sensitivity and transition metal dissolution [87]. Dopants can be utilized to enhance structural stability and delay oxygen evolution during thermal runaway [88]. Sustainable and abundant sourcing of carbon precursors can be employed for synthesizing HC anode materials. The use of highly compact HC particles would increase electrode density, resulting in decrease of electrode volume. This would use less flammable electrolyte, lowering safety risks. The first generation of sodium-ion batteries mostly use $NaPF_6$ salt with organic carbonates, while the upcoming variants could use advanced salts as $NaFSI$ salt forming inorganic SEI layer and less PF_5 gas generation [89,90]. An optimized set of additives to delay SEI breakdown, CEI protection for high voltage layered oxide materials, and flame-retardant additives can be used for advanced generation of sodium-ion batteries.

Table 1. Potential range and practical capacity of selected materials taken or deduced from mentioned sources of information.

Materials	Potential Range	Practical Capacity (mAh g ⁻¹)	Sources
Cathode:			
Li materials	vs. Li/Li ⁺		
Doped LiCoO ₂	3.0–4.5 V	190	[91]
LiNiO ₂	3.0–4.3 V	231	[92]
LiMnO ₂	3.0–4.3 V	210	[93]
LiNi _{0.33} Mn _{0.33} Co _{0.33} O ₂	3.0–4.3 V	164	[94]
LiMn ₂ O ₄	3.8–4.3 V	140	[95]
LiFePO ₄	≈3.45 V	150	[96]
Na materials	vs. Na/Na ⁺		
Na ₃ V ₂ (PO ₄) ₂ F ₃	2.0–4.2 V	120	[58]
NaFeO ₂	≈3.3 V	103	[97]
Na ₂ FeP ₂ O ₇	2.0–4.0 V	90	[98]
Na _{3.32} Fe _{2.11} Ca _{0.23} (P ₂ O ₇) ₂	2.2–4.0 V	100	[99]
Cutoff voltages:			
Na _{0.69} CoO ₂	4.3 V (Na _{0.12} CoO ₂), 4.1 V (Na _{0.24} CoO ₂), 3.5 V (Na _{0.52} CoO ₂)	147 (Na _{0.12} CoO ₂), 116 (Na _{0.24} CoO ₂), 49 (Na _{0.52} CoO ₂)	[100]

Table 1. Cont.

Materials	Potential Range	Practical Capacity (mAh g ⁻¹)	Sources
Na _{0.44} MnO ₂	2.0–4.0 V	108	[101]
NaNi _{0.33} Fe _{0.33} Mn _{0.33} O ₂	2.0–4.3 V	165	[102]
Na _{0.9} [Cu _{0.22} Fe _{0.30} Mn _{0.48}]O ₂	1.0–4.0 V	100	[103]
Na[Ni _{0.6} Co _{0.2} Mn _{0.2}]O ₂	2.0–4.1 V	153	[104]
Na _x Mn _y Fe(CN) ₆ ·nH ₂ O	3.3–3.8 V	67	[70]
Anode:			
Li materials	vs. Li ⁺ /Li		
Graphite	<0.4 V	348	[105]
Li ₄ Ti ₅ O ₁₂	≈1.5 V	160	[106]
Na materials	vs. Na/Na ⁺		
Hard carbon	0–1.5 V	361	[107]
Na _x Mn _y Mn(CN) ₆ ·nH ₂ O	1.7–2.5 V	68	[70]

The suitable choice of electrolyte, additives, and binders is equally as important as the choice of electrode materials for making safe and operational SiBs. The electrolyte and additives form a protective layer at both the cathode and the anode, designated as the Cathode Electrolyte Interphase (CEI) and the Solid Electrolyte Interphase (SEI) respectively [108]. Both these nanometric layers stabilize electrode–electrolyte interfaces [109,110]. Therefore, finding suitable electrolyte formulations is also crucial for developing high-performance SiBs, in terms of capacity, cyclability, and safety. Eshetu et al. [90] compared the SEI composition of sodiated hard carbons and lithiated graphite with X-ray photoelectron spectroscopy and found that the sodiated SEI possessed more organic species than lithiated graphite because of the lower Lewis acidity of Na⁺ (higher solubility) of inorganic sodium salts [111,112]. These results suggest that sodium cells have poorer SEI stability upon cycling, which poses problems of capacity retention and perhaps also of safety if we consider that the TR onset temperature corresponding to SEI degradation may be faster for SiBs than for LiBs. On the other hand, sodium salts are more thermally stable than lithium salts [113]; hence, lesser PF₅ and HF might be formed upon thermal decomposition of salt. This might delay or minimize the extent of TR when compared to LiBs; hence, this hypothesis of faster SEI decomposition but lower T_{max} reached during TR still needs confirmation from more global direct experimental comparisons of the two technologies.

When emerging technologies are changing constantly with research and development, the supply chain course might change overtime and influence the market share, hence investigating the safety of the latest technology must be carefully performed and reassessed as far as needed. This review introduces current research on materials and proposes future directions for sodium-ion batteries. On the other hand, despite developments in electrode materials and other components, there remain several challenges, including cell design and cell engineering in the application of sodium-ion cells; this paper will provide insights into the scientific and practical issues in the development of SiBs from the safety perspective.

Table 2. Selected commercial (start-ups) level sodium-ion batteries.

Company	Active Materials	Salient Features
Contemporary Amperex Technology Co., Ltd. (CATL), Ningde, China	Prussian white analogues HC	160 Wh/kg, charge in 15 min to 80% SOC at RT, capacity retention > 90% at -20 °C, thermal stability fulfills national safety requirement for traction batteries [114].

Table 2. Cont.

Company	Active Materials	Salient Features
Faradion Limited, Sheffield, UK	Layered oxide Materials $(\text{Na}_a\text{Ni}_{(1-x-y-z)}\text{Mn}_x\text{Mg}_y\text{Ti}_z\text{O}_2) \parallel \text{HC}$	160 Wh/kg in 32 Ah pouch cells, cycle life between 2300–3000 cycles at 78% DOD [115], possibility of zero volt discharge (negative voltages) [116], no flame or ignition detected during nail penetration tests [117].
HiNa Battery Technology Co., Ltd., Liyang, China	Layered oxide $(\text{NaCu}_{1-y-z}\text{Fe}_y\text{Mn}_z\text{O}_2) \parallel \text{Soft carbon}$	140–155 Wh/kg, 4500 cycles at 83% DOD (2C/2D), fulfills Chinese national standard GB/T31845-2015 [118], covering thermal, mechanical, and electrical abuse [119,120].
Natron Energy, Santa Clara, CA, USA	PBA ($\text{Na}_x\text{Mn}_y\text{Fe}(\text{CN})_6\text{.nH}_2\text{O}$) PBA $(\text{Na}_x\text{Mn}_y\text{Mn}(\text{CN})_6\text{.nH}_2\text{O})$	Zero strain during charge/discharge from –20 to 50 °C, over 50,000 cycles (23 Wh/kg at cell level and 10.3 Wh/kg at module level), no fire or explosion detected during mechanical and electrical mishandling [70,121,122].
TIAMAT, Amiens, France	Polyanionic material $(\text{Na}_3\text{V}_2(\text{PO}_4)_2\text{F}_3) \parallel \text{HC}$	100–120 Wh/kg, 10,000 cycles at 2C/5D, no thermal runaway observed during overheating, overcharging, nail penetration test, and short circuits [123].
Novasis Energies, Vancouver, WA, USA	PBA ($\text{Na}_x\text{MnFe}(\text{CN})_6\text{.nH}_2\text{O}$) HC	100–130 Wh/kg, nail penetration in fully charged cell causes temperature increase to 100 °C but no ignition was detected. On overcharging, the cells swell and temperature increases to 90 °C with no serious safety concerns [124].
Altris AB, Uppsala, Sweden	Prussian white analogues HC	160 Wh/kg, NaBOB salt-based electrolyte patented by Altris which is supposedly fire-resistant and complements PW cathode to improve electrochemical performance and safety [125,126].

A high-energy and high-power battery with targeted applications is desired but one should also equally anticipate its associated thermal and chemical threat. While considering SiB safety aspects, and given operational similarity between LiBs and SiBs, one should remember that incidents have paved the commercialization of LiBs since its infancy and that some myths regarding some safety aspects have had to be understood towards better safety considerations in developing electrochemical energy storage systems. Some misconceptions include that by the simple choice of adequate “safer” key materials selection (LFP cathode for instance), the TR problem would be solved; however, the fact is that the best choice will reduce the chance of TR but not eliminate it. Another myth is that selecting non-flammable electrolytes would solve the combustibility and release of toxic gases issues during TR; however, the definition of the non-flammability property is defined conventionally by regulators, may change versus time, and varies regionally. It does not replace field risk analysis considering strengths of potential ignition sources in terms of intensity and duration. Ionic liquids earlier thought to be non-flammable electrolytes due to their negligible vapor pressure have proven to be combustible as well [127].

From early scarce incidents reports of battery fires by the media, nowadays more structured and application-focused incident databases have come up like EV FireSafe platform or the EPRI Battery Electrical Energy Storage Systems (BESS) failure incident database [128,129]. This brings a new insight on the importance of the issue of sharp development of consumer market, as well as high power/energy demanding e-mobility and energy storage applications. Indeed, these structured databases help to learn lessons from past incidents in a scientifically sound manner [130]. Examples of some tragic incidents of battery failure include an EV bus with LiFePO₄ power batteries on fire in the charging

station in 2015 in Shenzhen, China [131]; Renault-Samsung's EV SM3.Z.E. catching fire from the front bonnet in 2016 in South Korea [132]; a large explosion and fire in a lithium battery warehouse in 2023 in Rouen, France [133]; and a fatal accident in South Korea in 2024 [134]. Indeed, fatal incidents involving LiBs have occurred throughout the full life cycle of batteries (from manufacturing to recycling), and in all types of applications from consumer market devices to large stationary applications. All these hazards correspond to the LiB failure, so will the possibility of a new SiB technology be a boon? It is a million-dollar question, with so far rather little to no answer in terms of consolidated evaluation, chiefly when considering the anticipated sharp innovation in the field as reflected by the increasing number of industrial promoters of variants of SiB technology. This was indeed a clear justification of this review work, focusing above all on unraveling this question [135]. Establishing what one knows currently on the matter as well as what needs to be further studied to accompany safe development of advanced versions of SiBs seems to be of the utmost importance. The active material and its potential associated menace could be tested at the component level, followed by cell level to module or pack design in due time for their safe and sustainable developments, two aspects that are from July 2023 key reinforced requirements in the EU since the publication of the new (EU) 2023/1542 Regulation on the matter [136]. This new EU Regulation [136] concerning the applications and repealing the old battery EU directive of 2006 sets new rules towards a safer and more sustainable battery value chain by considering the carbon footprint of battery manufacturing, ethical sourcing of precursors, and facilitating recycling.

2. Lessons to Be Learnt from LiBs to Develop Thermally Resilient SEI Layer in SiBs

Operational batteries form a nanometric SEI layer on the anode surface typically graphite for LiBs and hard carbons for SiBs. The formation of SEI layer is responsible for the irreversible capacity loss due to electrochemical reduction of electrolyte components during the primary cell cycles [137]. An ideal SEI is electronically insulating to prevent further electrolyte decomposition, and ionically conductive to selectively allow transport of Li^+ or Na^+ ions [138]. This layer must remain electrochemically stable and insoluble over the cycling course [139]. The composition of the SEI formed depends on the material surface chemistry and crystallography, the binder used, the composition of electrolytes (solvents, salts, and additives) and the electrochemical procedure adopted (current density, potentiostatic holds, temperature). The SEI formed in sodium-based electrolytes is reported to be less efficient than lithium counterparts with respect to self-discharge, probably due to the higher solubility of SEI components in sodium-based systems [112]. Na_2CO_3 and NaF , which are often the major components of Na-derived SEI, are reported to be more soluble in organic carbonate solvents than the corresponding Li_2CO_3 and LiF for Li-based SEI [111]. However, with appropriate electrode and electrolyte engineering, this issue could be tackled.

Additives are added to reinforce the SEI. The electrochemical stability window of the electrolyte is defined by oxidation (reduction) potentials related to HOMO (LUMO) levels of electrolyte and additives must lie within these levels [140]. Ideally, additives must have their LUMO energy levels lower than those of electrolyte solvents to reduce before and form an effective SEI layer [141], promoting the long cyclability of the cell. Out of solvents, mostly cyclic carbonates are primarily responsible for SEI formation [142]. Zhang et al. studied $\text{Na}_3\text{V}_2(\text{PO}_4)_3$ (NVP) || HC cells independently in EC and PC solvents and found that the generation of ethene and propene gaseous hydrocarbons corresponding to EC and PC reduction occurs around 2.6–3.1 V (ca. 0.8–0.3 V vs. Na^0/Na^+); moreover, EC solvent reduces on HC around 0.5 V vs. Na^0/Na^+ in half-cell [143]. Several researches have reported the use of additives such as vinylene carbonate (VC), sodium difluoro(oxalate)borate (NaODFB) [142,144], and fluoroethylene carbonate (FEC) reducing above 0.8 V vs. Na^0/Na^+ , which mitigate the decomposition of the electrolyte at the hard carbon electrode by forming an effective SEI layer as supported by DFT calculations. As the onset triggering point during TR is due to decomposition of the SEI layer [145], the

study of its thermal behavior is of great interest. These SEI-reinforcing reduction products could be thermally more resistant to breakdown at much higher temperatures [18].

Samigullin et al. [146] performed comparative studies of thermal stabilities for Li-ion and Na-ion electrode materials. The electrodes from a fully charged state were extracted from lithium and sodium corresponding half-cells comprising 1 M LiPF₆ in EC/DMC 1:1 and 1 M NaPF₆ in EC/PC 1:1 electrolyte, respectively, washed with DMC solvent, and dried under vacuum. These dried electrodes were placed in stainless steel crucibles for differential scanning calorimetry (DSC) analysis. The DSC profile obtained in Figure 1a for HC shows two broad peaks between around 150 and 300 °C. These peaks were assigned to SEI decomposition and redox reaction between sodiated HC and poly(vinylidene difluoride) (PVDF) binder.

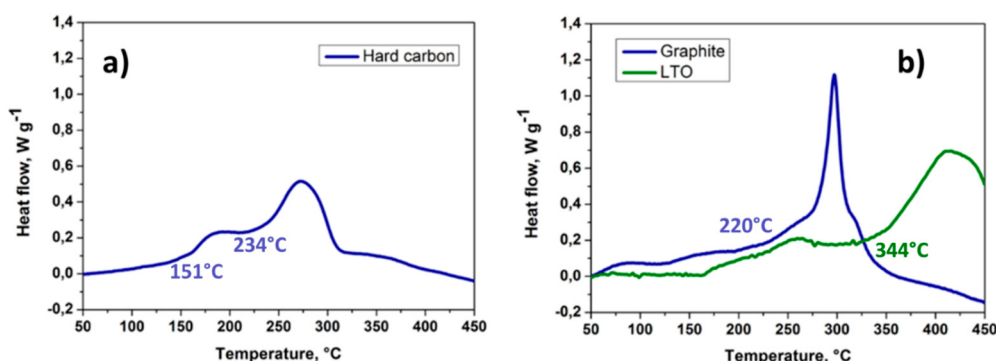
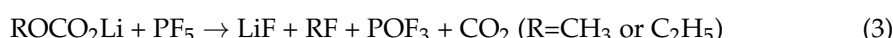
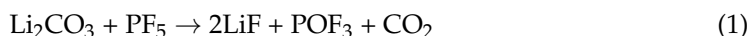


Figure 1. DSC profile curve of (a) Na-ion anode (hard carbon) and (b) Li-ion anode (graphite and LTO) after sodiation/lithiation. Reprinted with permission from [146]. Copyright 2022, American Chemical Society.

The authors said that the TR onset temperature of ~150 °C seems promising from safety point of view; however, as electrodes are washed, the first peak cannot represent the highly exothermic solvent reduction reactions consecutive to SEI decomposition, mostly responsible for the TR triggering. The DSC profile obtained in Figure 1b for lithiated graphite (LiC₆) shows a sharp peak around 297 °C (T_{onset} at 220 °C) corresponding to the redox reaction between LiC₆ and PVDF binder. The lithium–titanium spinel (Li₄Ti₅O₁₂) displays an almost flat DSC curve up to 350 °C and a broad peak around 420 °C with T_{onset} around 344 °C. This peak might correspond to the combustion of xerogel (solid material formed after evaporative drying of wet gel) precursor and release of CO₂ and H₂O gases [147].

The more realistic SEI breakdown for lithiated graphite was studied by Forestier et al. [18] who investigated its thermal behavior in presence of electrolyte. The exothermic heat of reaction was released in the temperature range from 100 °C to 325 °C as shown in Figure 2. The primary exothermic reaction between 100 and 250 °C was attributed to SEI breakdown and solvent reduction. The SEI breakdown was demonstrated to follow acid–base reactions [Equations (1)–(3)] between SEI components and PF₅ (LiPF₆ thermal decomposition product) [18].



It is interesting to compare the SEI breakdown in hard carbon for SiBs and if the thermal decomposition differs from one another. Eshetu et al. [113] studied the rate of exothermic heat release of carbonate mixture-based electrolyte with different Na salts, as shown in Figure 3.

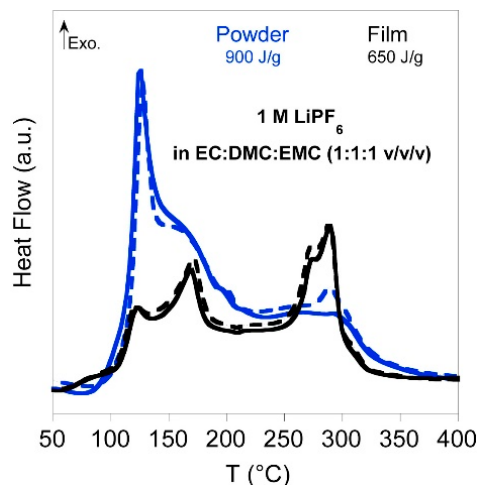


Figure 2. DSC profile of graphite/electrolyte after one lithiation. Reprinted with permission from [18]. Copyright 2016, Elsevier.

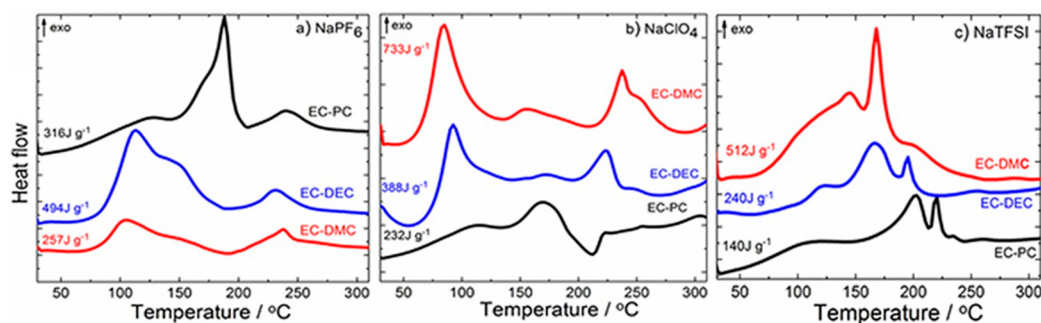


Figure 3. DSC profile of Na_x-HC electrodes with solvent mixtures and salt used: (a) NaPF₆, (b) NaClO₄, and (c) NaTFSI. Reproduced with permission from [113]. Copyright 2016, John Wiley and Sons.

Irrespective of the salt used, the solvent mixture EC/PC showed the lowest heat release, and therefore this mixture would be preferred for safer electrolyte formulation. EC/PC has an improved thermal property due to the intrinsic high polarity of both solvents where Na⁺ preferentially coordinates with both EC and PC [148]. For solvent mixtures, EC/DEC or EC/DMC, Na⁺ ions coordinate preferentially to EC and the linear carbonates DEC or DMC diffuse through the porous SEI layer to react with the highly reducing sodiated HC [113]. Even though the EC/PC solvent mixture appears to be a safe electrolyte, it must be noted that both are cyclic carbonates with high dielectric constant and high viscosity, hence for practical applications linear carbonates like DMC, DEC or EMC must be added to improve ion transport and ionic conductivity.

Information from DSC analysis regarding exothermic onset temperature linked to SEI breakdown, peak temperature, and overall heat generation enables researchers to compare and select safer electrolytes. The SEI layer formed is the result of the innate physico-chemical properties of the anode and the electrolyte used. Thus, by tuning the electrolyte composition, one can expect to some extent to delay the thermal runaway onset temperature. The similarity of the electrochemical processes between the two technologies lead us to take the example of the most advanced Li-ion technology for faster choice of electrolytes. However, in addition to the different nature of the anode material, the potentially higher solubility of the Na-SEI compounds and higher thermal stability of sodium salts compared to Li-counterparts make it challenging to predict the TR onset temperature based on results obtained from LIBs technology. Further in-depth thermal studies, combined with a detailed analysis of the composition of the SEI, are still required for both technologies to be able to anticipate any desirable change in reactivity.

3. Is Zero-Volt Storage Possible for SiBs and What Are the Added Safety Gains?

Sodium-ion batteries can use aluminum for the anode current collector instead of the copper used in LiBs. This change has an impact on over-discharge phenomenon, which is an electrical abuse that arises in cell module when there is a voltage imbalance between series-connected cells [149]. During the discharge of a Li-ion cell, the graphite-based anode potential vs. Li/Li^+ increases. As copper oxidizes at a potential greater than 3.5 V vs. Li/Li^+ , it is recommended not to discharge Li-ion batteries to 0 V to avoid reaching this copper dissolution potential [150]. Flügel et al. [151] discharged a commercial 18650 Li-ion cell, holding it at 0 V for 430 h, and observed that the current collector had visible holes by Cu dissolution. On recharging, the dissolved copper can form copper dendrites, which favors an internal short-circuit in the same way as lithium dendrite, inducing thermal runaway. On the other hand, as the copper current collector of LiB anodes is at around 3 V vs. $\text{Li}^\circ/\text{Li}^+$ in a just-assembled cell, the latter must be charged quickly after to move away from the oxidation potential of Cu, whereas SiBs can be stored appreciably after assembly without cycling.

With different chemistries and use of aluminum current collector for SiBs, the collector dissolution process does not occur in SiBs when discharged to 0 V. Rudola et al. [116] performed an over-discharge on a 5.5 mAh nominal capacity Na-ion pouch cell with a discharge rate of $C/2$; results are shown in Figure 4a.

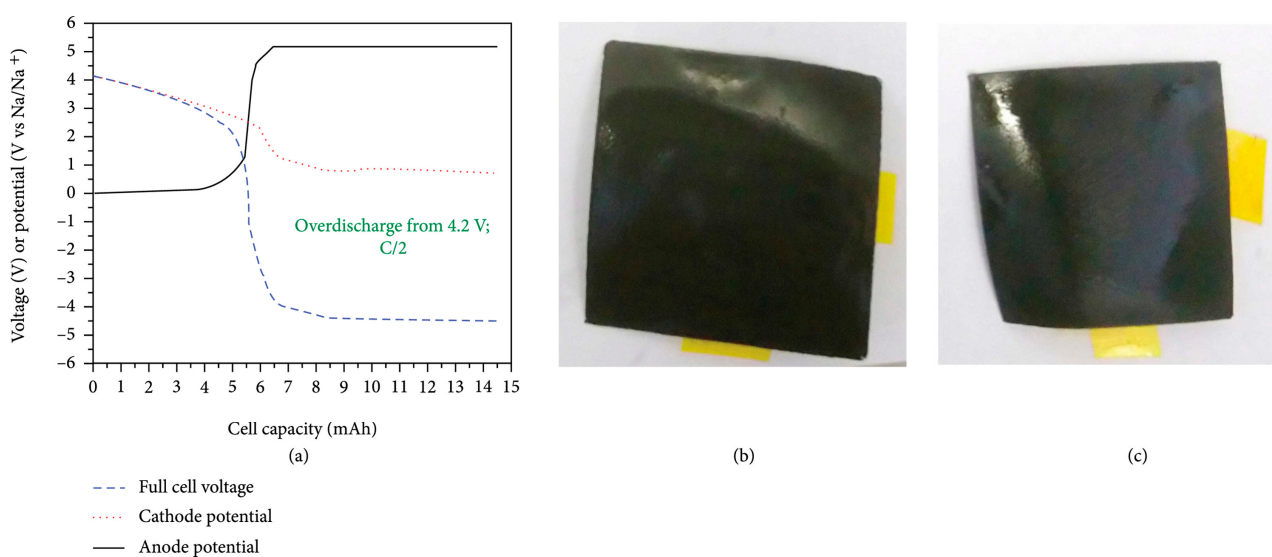


Figure 4. Effect of over-discharging Na-ion cells to negative voltages. (a) Cycling profile of three-electrode Na-ion cell. Pictures of the cycled (b) anode and (c) cathode. From reference [116] under CC BY 4.0.

To invigilate extreme worst conditions, the cell was discharged down to negative voltage so that the anode potential arose to 5.2 V vs. Na/Na^+ , a high potential well beyond the electrochemical stability window of organic electrolytes. The anode potential stayed at this value upon continued discharge due to electrolyte decomposition. As shown in Figure 4b,c, no visible decomposition products are observed on anode and cathode surfaces. Another similar study performed by Rudola et al. [152] shows the cycling profile of a Faradion Na-ion cell fully discharged down to 0 V and held at this potential for 24 h (Figure 5a). The cycling stability of this cell cycled between 4.3 and 0 V and held at this low voltage for 24 h after each cycle (Figure 5b) is not compromised. Considering the above, the zero-volt storage possibility in SiBs might be a boon for safe transportation.

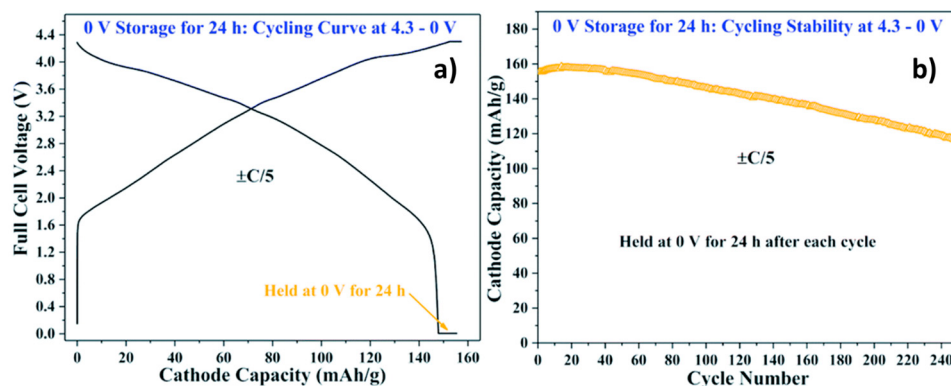


Figure 5. (a) Cycling curve of Faradion Na-ion cell discharged down to 0 V and potentially held for 24 h. (b) Cycling stability when the cell is cycled between 4.3 and 0 V and held at this low voltage for 24 h after each cycle. Reproduced with permission from [152]. Copyright 2021, Royal Society of Chemistry.

The large demand for electronic devices requires them to be shipped worldwide either by land, air and sea. LiBs are classified under United Nations (UN) category 9 as dangerous goods because they are thermally and electrically unstable when exposed under certain uncontrolled environmental conditions or mishandled during transportation [153]. Hence, when transported, these batteries must follow the applicable regulations according to their mode of transportation: The European agreement concerning the international carriage of dangerous goods by road (ADR), the international carriage of dangerous goods by rail (RID), the international civil aviation organization (ICAO) technical instructions for the safe transport of dangerous goods by air, the international air transport association (IATA) dangerous goods regulations, the international maritime dangerous goods code (IMDG code) for sea transportation, and so on [154]. The higher the SOC during transport, the greater the risk of explosion and thermal runaway. Therefore, during transportation, a lower SOC is recommended; however, LiBs have serious complications when discharged down to 0 V, as discussed above. A fully charged battery represents the most thermally unstable state. He et al. [155] studied the effect of SOC on the self-heating behavior of $\text{LiCoO}_2 \parallel$ graphite prismatic cells. The cells were heated in a mechanically ventilated oven and the presence of flames was detected at $\text{SOC} \geq 80\%$. Hence, transportation of batteries must be strictly prohibited at such high SOC. Hence, to ensure safety and save lives, the ICAO and the IATA have issued statements prohibiting the transport of Li-ion cells and batteries at SOC exceeding 30% [156,157]. With the emerging sodium-ion powered batteries, the ICAO has published a joint statement for vehicles powered by SiBs (UN 3558) in addition to LiBs (UN 3556) and lithium metal batteries (UN 3557). Vehicles must have the battery(ies) discharged as far as practicable, and where charge remains, the capacity must not exceed 25% SOC [158] for safe transportation. UN numbers are assigned to each dangerous goods and shipping names based on their hazard classification and composition. LiBs and SiBs are classified into Class 9, and assigned as UN numbers 3090, 3091, 3480, 3481, and 3536 and UN numbers 3551 or 3552, respectively [159]. These four-digit numerical codes designate specific dangerous goods for transport, according to the type of hazard class. It defines provisions for transport in terms of packaging instructions, potential limited quantities per package, and special provisions for transport. Additionally a special provision uniquely for SiBs assigned as UN 3292 allows the transportation of shorted or discharged sodium-ion batteries after sufficient evidence that the electrical or mechanical abuse during its transport do not bring about serious safety hazards [160]. As shown in Figures 4 and 5, zero-volt storage might be a possibility for SiBs [116,152]. However with discrepancies and arguments among researchers, Desai et al. [161] showed that zero-volt storage of SiBs is heavily dependent on cathode cell chemistry and the electrolyte used, and is not an innate property for all SiBs. Hence, more advanced studies must be performed to unravel the true zero-volt storage possibility for SiBs.

4. Comparative Thermal Studies of SiBs Versus LiBs

4.1. Component Level

4.1.1. Cathode Material

Layered intercalated oxide compounds are used as one of the cathode families for both high-energy SiBs and LiBs. Zhao et al. [97] investigated the electrochemical and thermal property of an O3-type layered material, α -NaFeO₂ for SiBs and compared it with LiCoO₂ cathode material of LiBs. Na_{0.58}FeO₂ was formed at the end of the first charged cycle. ⁵⁷Fe Mössbauer spectrometry confirmed the presence of Fe⁴⁺ super iron state on charging making α -NaFeO₂ the first iron-based cathode active material based on Fe³⁺/Fe⁴⁺ redox couple. Cobalt is acutely more toxic than iron hence the use of iron-based Na cathode material is a favorable choice for safer material selection. Further, to check cathode material thermal stability, the desodiated Na_{0.58}FeO₂, and delithiated Li_{0.5}CoO₂ powders were tested by DSC as shown in Figure 6.

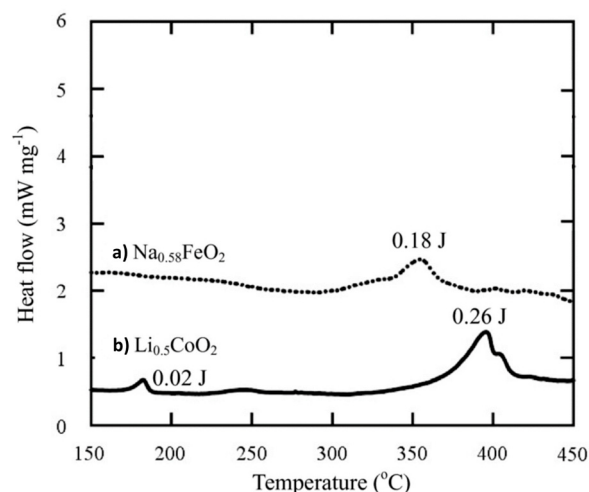
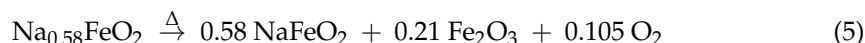
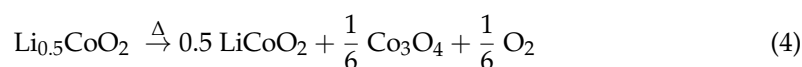


Figure 6. DSC curves of washed with DMC and dried (a) desodiated Na_{0.58}FeO₂ cathode powder and (b) delithiated Li_{0.5}CoO₂ cathode powder after two cycles. Reproduced with permission from [97]. Copyright 2013, IOP Publishing.

Figure 6a showed an exothermic peak at 360 °C detected for Na_{0.58}FeO₂ desodiated cathode because α -NaFeO₂ became thermally unstable due to the generation of Fe⁴⁺ abnormal valence state. Li_{0.5}CoO₂ powder in Figure 6b showed two exothermic peaks at 190 and 395 °C. Those peaks would correspond to the phase transitions from layered rocksalt to spinel and/or rocksalt structures accompanied with oxygen release [37,162]. Thus, suspected similar reactions were supposed to take place for the two materials as shown in Equations (4) and (5).



Comparing Na_{0.58}FeO₂ and Li_{0.5}CoO₂ materials at charged state, the Na cathode shows better thermal stability, no phase transition as for Li cathode, higher T_{onset}, and lower heat generation. These findings prove that Fe-based Na-ion layered cathode is of higher interest than Co-based Li-ion layered cathode in terms of cathode safety. Zhao et al. [97] further studied the thermal behavior of these cathode materials in the presence of electrolyte, as shown in Figure 7, by keeping constant the charged active material or the electrolyte mass.

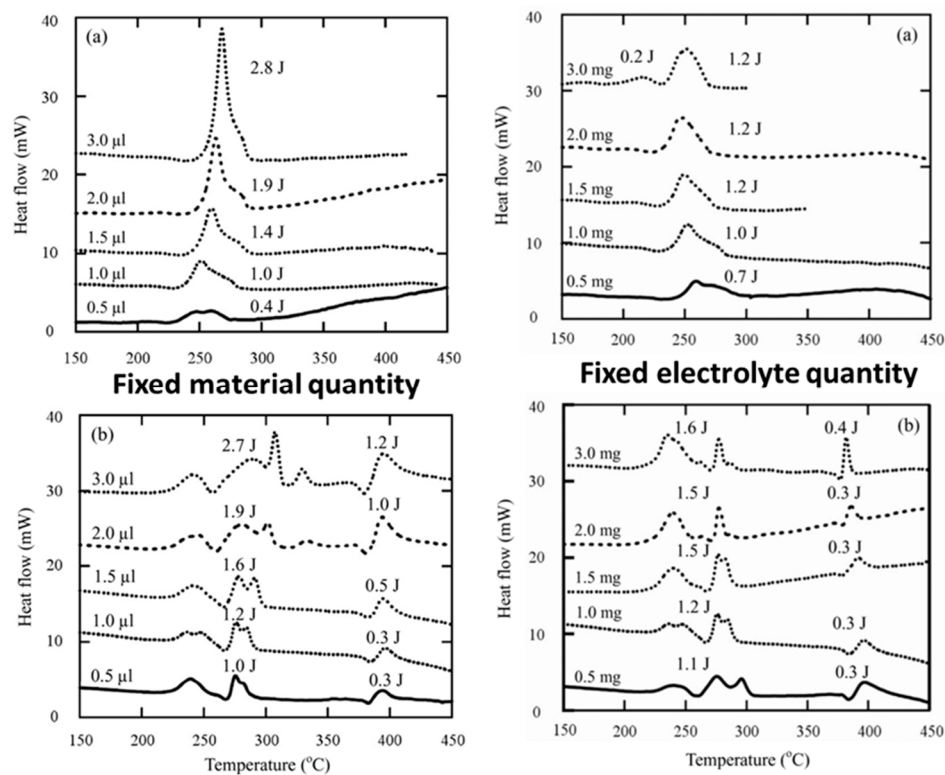
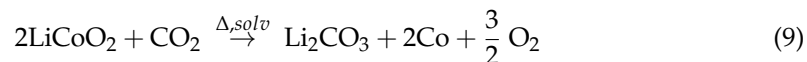
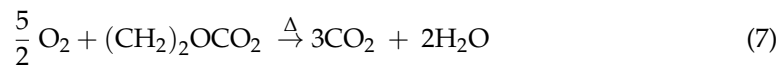


Figure 7. DSC curves for fixed material quantity: (a) 1 mg of Na_{0.58}FeO₂ powder mixed with electrolyte and (b) 1 mg Li_{0.5}CoO₂ mixed with electrolyte. Fixed electrolyte quantities: (a) given amount of Na_{0.58}FeO₂ powder mixed with 1 µL of electrolyte and (b) given amount of Li_{0.5}CoO₂ powder mixed with 1 µL of electrolyte. Reproduced with permission from [97]. Copyright 2013, IOP Publishing.

As observed in Figure 7, the Na and Li layered oxides showed contrasting DSC profiles. For the Na cathode (Figure 7a, fixed material quantity), on increasing electrolyte quantity from 0.5 µL to 3 µL, the exothermic peak increases and slightly shifts to higher temperature. This suggests that the heat generation is mainly due to the electrolyte thermal decomposition. The mechanism of heat generation from Li_{0.5}CoO₂ with electrolyte has been studied well. Co₃O₄ is formed when Li_{0.5}CoO₂ oxygen evolution takes place as shown in Equation (4). The following are the chain reactions generated from Co₃O₄ and EC solvent as shown in [Equations (6)–(9)] which have been studied by MacNeil et al. by calorimetric techniques (DSC, ARC) and XRD [163,164].



These series of reactions take place for Li_{0.5}CoO₂ with electrolyte from temperature range of 200 to 430 °C, hence their DSC curve (Figure 7b, fixed quantity) appears more complicated than the Na-ion counterpart. Fe₂O₃ formed in Equation (5) from thermal decomposition of the Na cathode might possess improved thermal stability as compared to Co₃O₄ to prevent the cascading chain of reactions. Hossain et al. [165] investigated the thermal stability of Fe₂O₃ with carbonaceous spheres and TGA/DTA analysis confirmed

that an exothermic peak at 462 °C was detected due to the decomposition of $\gamma\text{-Fe}_2\text{O}_3$ to $\alpha\text{-Fe}_2\text{O}_3$ [166]. The calcined hollow $\alpha\text{-Fe}_2\text{O}_3$ exhibited no weight loss until 1000 °C, validating the high thermal stability of the compound. This delayed thermal response of Fe_2O_3 could attribute to the added safety gain.

Zhao et al. [97] studied alternative configuration with varying amounts of $\text{Li}_{0.5}\text{CoO}_2$ and $\text{Na}_{0.58}\text{FeO}_2$ charged material with 1 μL of electrolyte, the results are shown in Figure 7 (fixed electrolyte quantity, a and b). As before, $\text{Na}_{0.58}\text{FeO}_2$ shows simpler DSC curves than $\text{Li}_{0.5}\text{CoO}_2$ cathode. The increase in the cathode content mildly increases heat generation but retains peak shape and no major temperature shift is observed from both Li- and Na-based cathode. The Na cathode gives off less heat generation in this orientation which is recommendable from safety viewpoint and overabundant cathode had no drastic contribution to heat increase.

Barpanda et al. [98] studied the polyanionic insertion cathode compound, $\text{Na}_2\text{FeP}_2\text{O}_7$ pyrophosphate. The desodiated cathode composition after charging to a potential of 4 V vs. Na/Na^+ was $\beta\text{-NaFeP}_2\text{O}_7$. The thermal stability of this charged phase was measured by TG-DSC technique. An exothermic peak with onset temperature of 564 °C and heat generation of 16 kJ mol^{-1} was obtained as shown in Figure 8. The TG curve showed no weight change which inputs the high thermal stability of $\beta\text{-NaFeP}_2\text{O}_7$. Temperature dependent XRD analysis on the charged cathode revealed that at 560–580 °C an irreversible phase transition from $\beta\text{-NaFeP}_2\text{O}_7$ (triclinic, $\text{P}\bar{1}$) to $\alpha\text{-NaFeP}_2\text{O}_7$ (monoclinic, $\text{P}2_1/\text{c}$) had taken place. This complements the DSC result and answers the exothermic peak generation at 564 °C. The inherent high stability of pyrophosphate ($\text{P}_2\text{O}_7^{4-}$) units could be the reason for high thermal stability. Liu et al. [99] also studied the stability of $\text{Na}_{3.32}\text{Fe}_{2.11}\text{Ca}_{0.23}(\text{P}_2\text{O}_7)_2$, which falls under pyrophosphate-based Na cathode and observed similar phase transition from triclinic to monoclinic phase with enhanced thermal properties. Additionally, Ca-doping in this study enhanced the material's thermal stability, hence doping could be a good strategy to enhance both capacity retention and structural stability. These researches help promote safe cathode development for sodium-ion battery technology.

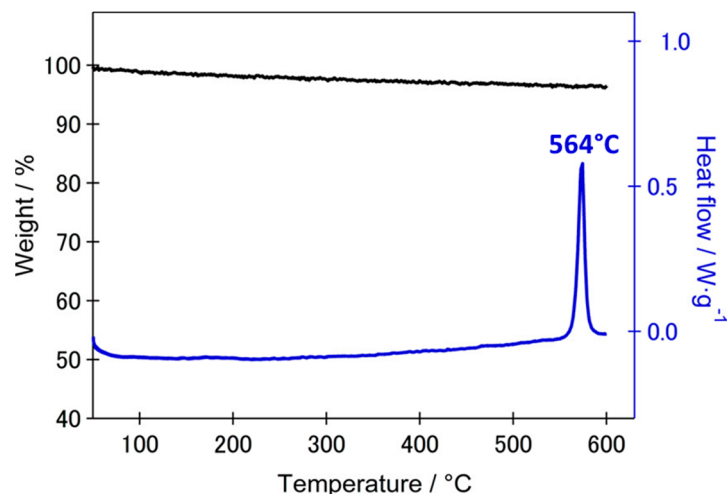


Figure 8. Thermal analysis (TG–DSC) curves of the desodiated NaFeP_2O_7 phase under Ar flow. Reprinted with permission from [98]. Copyright 2013, American Chemical Society.

The structural changes of active material and thermal stability may depend on SOC or sodiation/lithiation levels. Hwang et al. [100] performed constant charge experiments for layered oxide P2-type $\text{Na}_{0.69}\text{CoO}_2$ cathode material versus Na metal until the cut off voltages reached 3.5, 4.1, and 4.3 V. These led to the formation of $\text{Na}_{0.52}\text{CoO}_2$, $\text{Na}_{0.24}\text{CoO}_2$, and $\text{Na}_{0.12}\text{CoO}_2$ charged states, respectively. The local changes in crystallographic, electronic structures and morphology of charged P2-type Na_xCoO_2 cathode with temperature ramp was studied using real-time in situ TEM microscopy. The morphology change of NCO materials was tracked by recording bright field images from room temperature to 400 °C.

As shown in Figure 9, the NCO morphologies were more severely affected for charged materials at higher SOC and exposed to higher temperatures, likely due to the complicated series of phase transitions of layered oxide materials at these voltages.

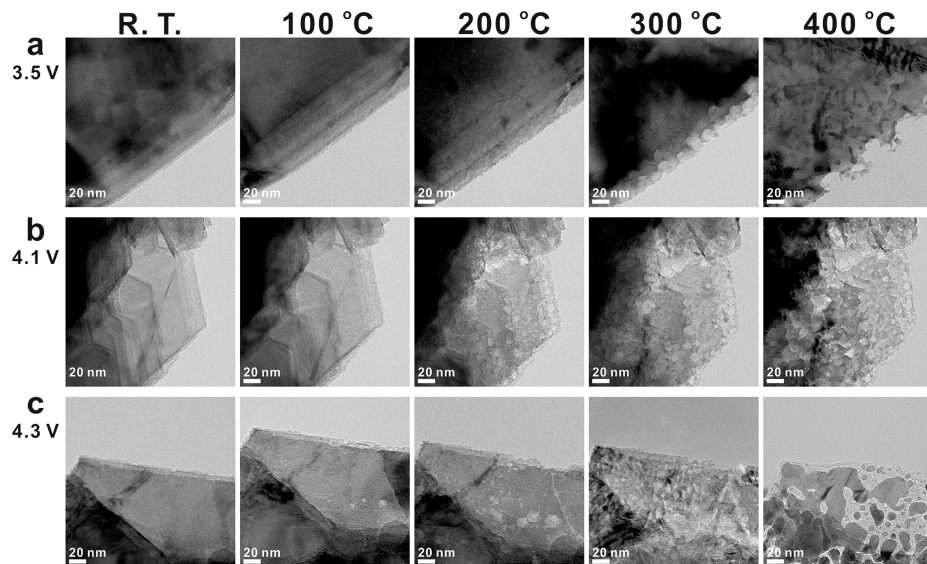


Figure 9. Real-time bright-field images of NCO cathode surface charged to (a) 3.5 V, (b) 4.1 V, and (c) 4.3 V during heating. Reprinted with permission from [100]. Copyright 2017, American Chemical Society.

The crystal phases corresponding to each temperature were determined from selected area electron diffraction (SEAD) patterns. The desodiated Na_xCoO_2 cathode decomposed to Co_3O_4 and CoO or metallic Co at very high temperatures. The Co_3O_4 phase was found only at 400 °C for the sample charged to 3.5 V; on the contrary, the Co_3O_4 phase was found even at 100 °C for those samples charged to 4.3 V. For the harshest condition of 4.3 V and 400 °C used in this study, significant morphology changes, as well as reduction of cobalt oxide to a metallic state and loss of oxygen from the structure were observed. These are serious threats to the battery system; one needs to go to high voltages (here 4.3 V) to access the maximum capacity to store more energy, but reaching high voltages seems detrimental from thermal runaway point of view. Hence, in the quest for finding SiBs with enhanced electrochemical performances, it is crucial to find a balance between producing high-energy or -power batteries and safety managements constraints.

The first commercial Prussian blue || HC-based sodium-ion battery was exposed to internal short-circuit, mechanical, electrical, and thermal abuse tests to verify its safety limits [70]. These cells do not show thermal runaway behavior nor flame, or explosions based on the standard UL 9540A (Fire safety hazards associated with propagating thermal runaway within battery systems) test irrespective of the testing circumstances. However, out of the three cathode families of SiBs, sodiated layered transition metal oxides, polyanionic materials, and Prussian blue analogues, it is interesting to note the advantages and safety differences that have been reported in Table 3. Layered oxides generally have the highest energy density because they typically operate at higher voltages (>3.6–4.3 V vs. Na/Na^+) and possess higher specific capacities than other cathode families. However, they are more prone to oxygen loss from their structure, and thus poor structural stability with temperature increase. Polyanionic compounds have strong covalent bonding between the transition metal and the polyanionic groups, which is typically stronger than the M-O bonds in layered oxides [167]. Hence, polyanions feature the least thermal runaway behavior. The possible toxic gases emission from sodium-ion batteries (irrespective of cathode type) can include CO_2 , CO , CH_4 , C_2H_4 , organic carbonates, H_2 , and so on. However, under extreme conditions, Prussian blue analogues can supply supplementary asphyxiants like HCN and cyanogen gas [74,75].

Table 3. General comparison of sodium-ion cell with different cathodes.

	Layered Oxides	Polyanionic Materials	Prussian Blue Analogues
Energy density of cell	😊	😐	🙁
Structural stability of material	🙁	😊	😐
Toxic gases emission from cell	😐	😐	🙁
Thermal runaway density of cell	🙁	😊	😐

4.1.2. Electrolytes

Zhao et al. [168] studied the thermal stability of Na electrolytes and compared with Li electrolytes with TG-DSC technique. The thermal stability of electrolytes is dominated by the solvent used. NaClO_4 and NaPF_6 salts were tested in both EC-DMC solvent mixture and PC solvent with the corresponding synonym formulation for Li-electrolytes as shown in Figure 10. The results show that the PC-based solvent generated larger heat of formation than EC-DMC-based solvents; however, the average onset temperature for EC-DMC solvents is about 25 °C lower than PC-based solvents. These studies also reveal that Na-salt electrolytes generate around the same heat and increased onset temperature (ca. +20–50 °C) than corresponding Li-salt electrolytes. This explains the better thermal stability of Na-salt electrolytes, which provides improved safety in case of thermal runaway.

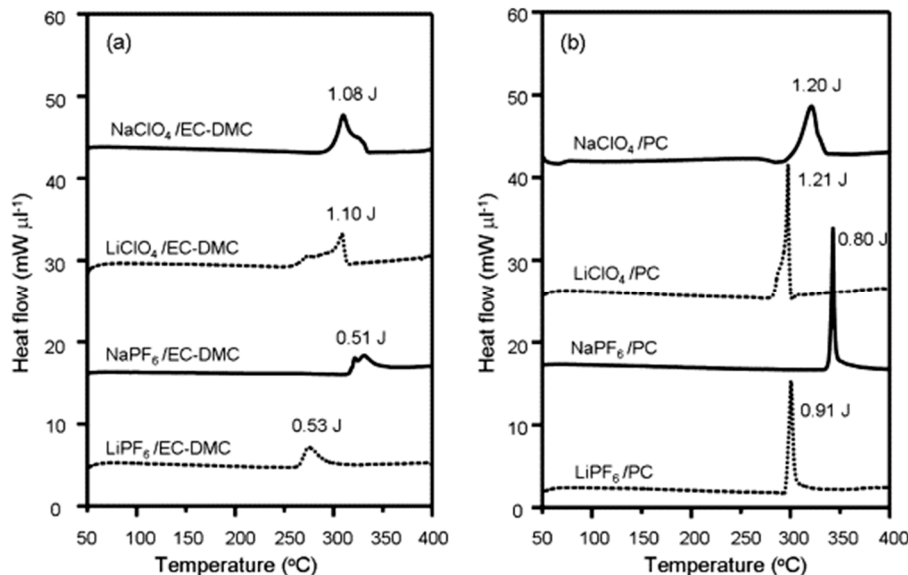


Figure 10. DSC curves for different Na- and Li-salt electrolytes using (a) EC-DMC solvents, and (b) PC solvent. Reproduced with permission from [168]. Copyright 2013, Elsevier.

Eshetu et al. [113] studied the thermal reactivity of Na-based salts by TG analysis and showed that Na salts are much more thermally stable than corresponding Li salts. As shown in Figure 11, the thermal stability of the Na salts decreases in the order of $\text{NaClO}_4 > \text{NaTFSI} > \text{NaPF}_6 > \text{NaFTFSI} > \text{NaFSI}$. Even though NaClO_4 outperforms other salts, it is generally a strong oxidizing agent and explosively decomposes over 130 °C in the dry state [169]. Hence, its use must be limited and exploring other alternatives are recommended. A comparison between LiPF_6 and NaPF_6 salts indicates that their decomposition starts around 125 and 325 °C, respectively; this is true for most of the

equivalent Li and Na salts. Na salts are much more stable than the homologous Li salts, explained by higher Madelung energy, a parameter linked to the electrostatic energy in ionic crystals. Moreover, as obtained in Figure 11, LiPF₆ salt loses ~83% of its mass at 250 °C, whereas NaPF₆ salt does not show observable change up to 300 °C. It is worth noting that the thermal degradation of Li(Na)PF₆ leads to the formation of the Lewis acid PF₅, which adversely reacts towards the basic salts of the SEI in batteries or water from environmental air to yield HF. In addition to the gain in intrinsic safety, these results also indicate that SiBs might perform better than LiBs in long-term capacity retention and storage at high temperature, which could be one of the potential applications of the emerging SiBs.

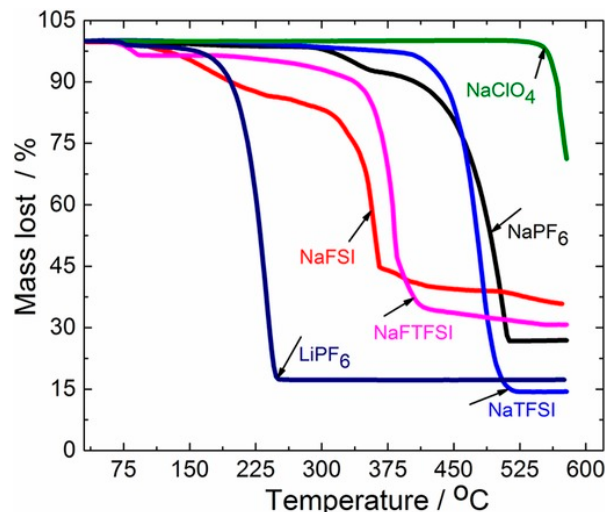


Figure 11. TGA profiles of Na salts: NaPF₆, NaClO₄, NaTFSI, NaFTFSI, and NaFSI, and the state-of-the-art LiPF₆ salt in LiBs. Reproduced with permission from [113]. Copyright 2016, John Wiley and Sons.

The fire hazards of carbonate electrolytes for sodium-ion and Li-ion batteries have been compared with Fire Propagation Apparatus [170]. The thermal threat of classical LiPF₆ and NaPF₆-based electrolytes remains quite similar as the heat release rate profile is dominated by the equivalent cyclic (EC) and linear (DMC) carbonate solvents used. However, the fate of chemical threats (HF and POF₃ toxic gases released) favors sodium-ion electrolytes safety, as shown in Table 4. These asphyxiant gases are emitted in lesser quantities by sodium-ion electrolyte. This is because of the greater thermal and hydrolysis stability of NaPF₆ salt which induces slighter PF₅ generation giving off lesser HF and POF₃ production through reaction with water, mainly originating from the combustion of the carbonates. The sodium salt prefers to stay in residue form after combustion unlike the LiPF₆ which gives off more hazardous emissions. Moreover, the toxic gas emissions of advanced sodium-ion carbonate electrolytes containing NaFSI salt (with additives) remains inferior to classical Li-ion electrolytes.

Table 4. Chemical quantification of gases released from burning carbonate electrolytes for Li-ion and Na-ion batteries. From reference [170] under CC BY 4.0.

Gases Emitted (mg/g of Electrolyte Burnt)	HF	POF ₃
EC/DMC (1:1 wt. ratio) LiPF ₆ 1 M	59.1 ± 0.7	25.5 ± 1.1
EC/DMC (1:1 wt. ratio) NaPF ₆ 1 M	16.5 ± 0.5	1.2 ± 0.1

Careful selection of flame retarding additives also promotes overall cell safety. Feng et al. [101] used an ethoxy(pentafluoro)cyclotriphosphazene (EFPN) additive and investigated the flame-retarding efficiency with the base electrolyte, 1 M NaPF₆ in EC:DEC solvent mixture. The resilience to flaming combustion hazard of the electrolyte was studied by

so-called self-extinguishing time (SET). Figure 12 shows the variation in SET and ionic conductivity of the electrolyte with increasing EFPN content. The SET value dropped from 58 s to 0 s with no EFPN to 5 wt% of EFPN additive, hinting that the electrolyte transformed from ‘flammable’ to ‘non-flammable’ in these specific test conditions. The more global fire hazard needs some more careful consideration however, since it will be assessed according to potential activation energy sources, which in the domain of batteries may rank well over ignition sources used to qualify flammability of liquid chemicals referring to the flash point measurements for regulatory purposes [171]. The ionic conductivity of the electrolyte decreased from 6.4 mS cm^{-1} to 5.7 mS cm^{-1} and then to 4.6 mS cm^{-1} when EFPN content increased from 0 to 5 wt% and then to 15 wt%. Thus, it is also important to find an optimum between SET and conductivity. With 5% EFPN additive in the base electrolyte, the electrochemical performance of $\text{Na}_{0.44}\text{MnO}_2$ cathode and acetylene black anode improved as well.

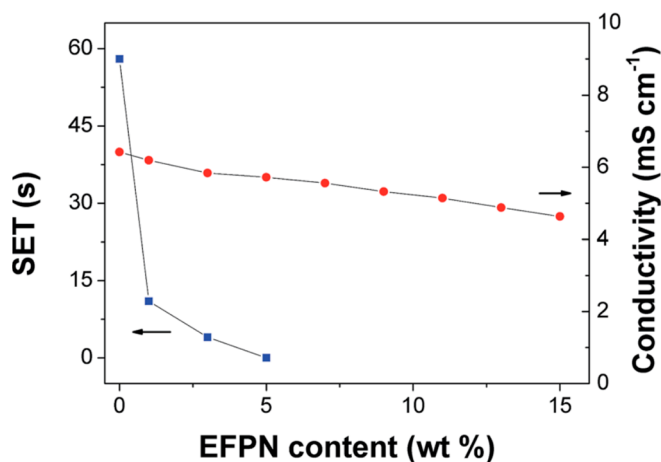


Figure 12. Flammability and ionic conductivity of 1 M NaPF_6 /EC-DEC (1:1, *v/v*) at different EFPN additive contents. Reproduced with permission from [101]. Copyright 2015, Royal Society of Chemistry.

Yang et al. [172] studied the effect of 1.2 M sodium bis(trifluoromethanesulfonyl) imide-trimethyl phosphate/bis(2,2,2-trifluoro ethyl) ether/vinylene carbonate electrolyte (1.2 M NaTFSI-TMP/BTFE/VC) with electrode contact to analyze the flammability behavior. It was compared to the classical electrolyte 1 M NaPF_6 in EC/DEC, which is flammable, as shown in Figure 13a, and possesses poor compatibility with electrodes due to continual electrolyte decomposition and poorer passivation film protection of electrodes. In comparison, 1.2 M NaTFSI-TMP/BTFE/VC shows improved resilience to flaming combustion (Figure 13b) due to the dispersed concentrated salt-solvent clusters by fluorinated BTFE ether. Hence, according to the fire test selected, it seemed to develop some fire-retardant properties with the proposed electrolyte. However, this kind of fire testing is not well recognized in the field of battery testing, and ‘non-flammability’ claims (speaking about non-intrinsic material property) may be misleading in terms of real ignitability and combustibility. Next, pouch cells with sodium-vanadium phosphate || HC and Prussian blue || HC were cycled with the fluorinated electrolyte and used to investigate the safety of the whole system using the flame test by simultaneously powering a light bulb, as shown in Figure 13c. The edge of the cell was cut and even though it was exposed to air, the bulb kept on glowing. As the cells burnt, no smoke or fire was emitted in these test conditions. The post-mortem results verified only the part that was in direct contact with flame was damaged, while the other parts remained intact. This was attributed due to the improved flame-retarding properties of the electrolyte. Thus, tuning electrolyte properties helps to produce safer sodium-ion batteries, and such approaches must be promoted for advanced formulations.

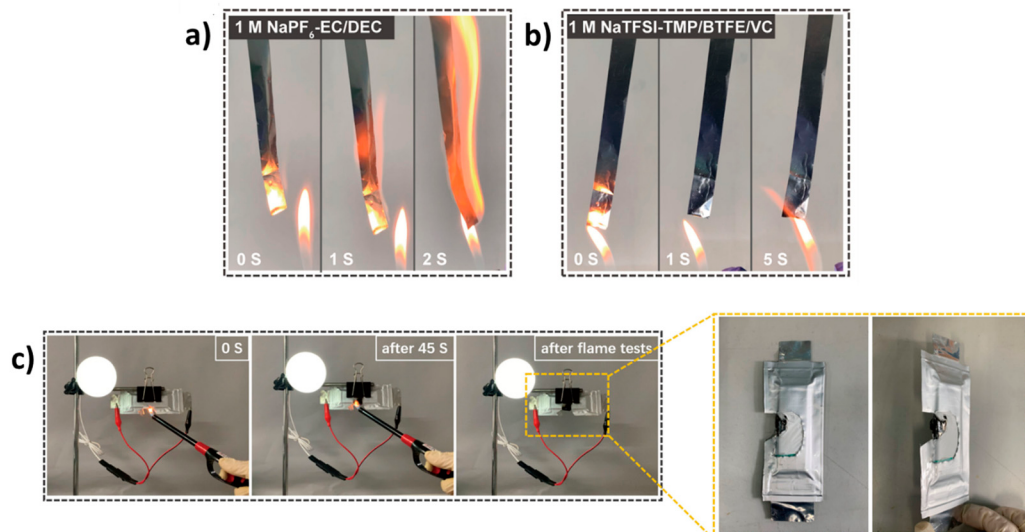


Figure 13. Flammability tests for (a) 1 M NaPF₆-EC/DEC electrolyte and (b) 1.2 M NaTFSI-TMP/BTFE/VC electrolyte. (c) Flammability tests on the pouch cells and the post-mortem dissection of the burned cell. Reproduced with permission from [172]. Copyright 2021, John Wiley and Sons.

Different flame-retardant additives have been previously used on lithium-ion batteries to promote overall battery safety. These additives work via different approaches: trapping of highly reactive free radicals produced during combustion [173] by phosphate-based radicals, formation of protective interfacial layer on the material's surface inhibiting diffusion of heat [174], or by improving the thermal stability of the electrolyte [175]. Some of the additives are listed in Table 5. These families of additives must be promoted in the blooming SiBs to promote overall cell security. Flame retardant polymer electrolytes for sodium-ion battery applications have been proposed [176,177] and further research on these grounds should be encouraged.

Table 5. Some flame-retardant additives for LiBs.

Cell Chemistry	Base Electrolyte	Additive(s)	Safety Improvement
LiNi _{0.8} Co _{0.2} O ₂ Graphite	1 M LiPF ₆ in 1:1 EC:DEC	Triphenylphosphate (TPP) and Tributylphosphate (TBP)	Underwriters Laboratories (UL) test standard 94 showed, with TPP additive, decreased flame propagation rates. ARC experiments on charged graphite electrode and electrolyte with TPP or TBP additives demonstrated lower exothermic heat generation [178].
LiNi _{0.8} Co _{0.2} O ₂ Li	1 M LiPF ₆ in 1:1 EC:DMC	Hexamethoxycyclotriphosphazene ([NP(OCH ₃) ₂] ₃)	Thermal stability of fully lithiated graphite electrolyte with additive decreased the overall heat of production. ARC results showed that the maximum self-heating profile of electrolyte without and with additives improved from 0.68 °C/min to 0.19 °C/min respectively [179].
LiMn ₂ O ₄ : Li(Ni _{1/3} Co _{1/3} Mn _{1/3})O ₂ (8:2) Li ₄ Ti ₅ O ₁₂	1 M LiPF ₆ in 1:2 EC:EMC with 2% VC	3,3',5,5'-tetrabromobisphenol A (TBBA)	Safety tests were performed on 100% SOC charged 18650 cells developed on in-house safety procedure. The cells with TBBA additives had flame-retardant (self-extinguishing) ability even at 1 wt% of TBBA content [180].

4.2. Full Cell Level

The French National Institute for Industrial Environment and Risks (INERIS) performed thermal runaway of 18650 type NVPF || HC cells commercialized by TIAMAT [181]. These Na-ion cells were charged to full SOC and then thermal runaway was triggered with homemade built system by overheating with four cartridge heaters (400 W each) integrated into copper block with calibrated holes. Six identical cylindrical cells were tested independently, and as the heaters were switched on, the TR was observed when the temperature increased exponentially, as shown in Figure 14. The time between the six cells that went into TR first (Temp 1) and in the end (Temp 4) was shorter than 15 s. The maximal average recorded temperature was 286 °C, with the degassing process from white fumes lasting no longer than 40 s. The gas analysis from these cells was simultaneously performed and the EMC solvent due to its volatile nature from electrolyte source showed the most abundant release during the same time of TR. The other released gases were PC, EC, H₂, CO₂, CO, CH₄, C₂H₄, and HF. HF accounted to only 4 vol % of the total release which demonstrated limited toxicity originating from Na cells. Additionally, it showed no traces of POF₃ toxic gas, which is a common toxic hazard during LiBs thermal runaway.

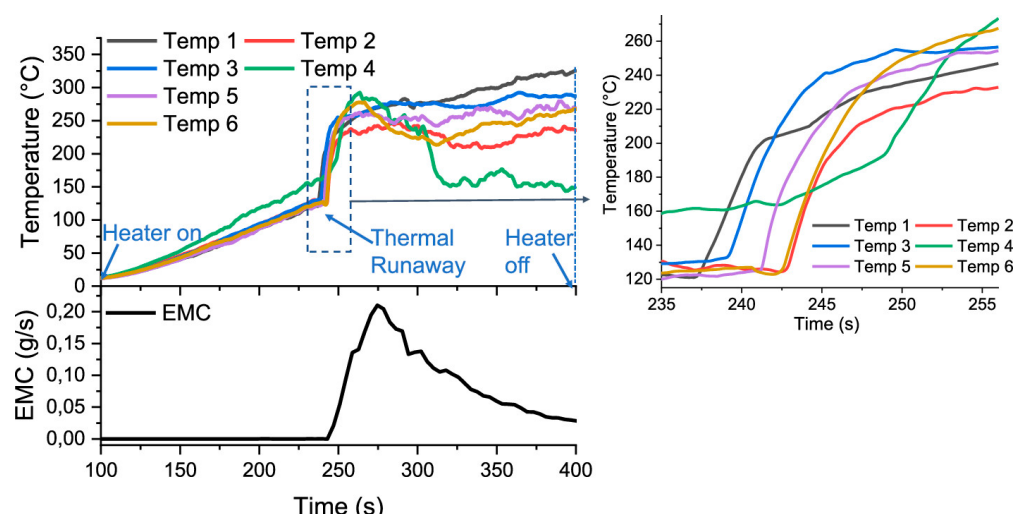


Figure 14. Evolution of temperature of NVPF/HC cells on heating with cartridge heaters. Reprinted with permission from [181]. Copyright 2022, American Chemical Society.

To compare these results with those of LiB technology reported in the literature, the methods employed, and the protocol analysis of TR must be consistent for fair differentiation. The comparable results for LiBs with non-flaming combustion were observed for the safer low nickel content layered oxide LiNi_{1-x-y}Mn_xCo_yO₂ (NMC111 with $x = y = 0.33$) || graphite and LiFePO₄ (LFP) || graphite cell technologies when abused thermally by internal heater or overcharged [182,183]. The LFP and NVPF phosphate-based cathodes gave off mostly similar gases. However, PF₃ gas was additionally observed in LFP cell abuse which was absent in NVPF chemistry. The NMC111 cells had some differences in gas generation from NVPF chemistry. The organic carbonates were present in lesser quantities in NMC111 cell, but this was balanced by increasing amounts of CO₂ and CO gases. This difference was due to the readiness of oxygen release in NMC cathode than NVPF and LFP chemistry.

The work performed by Yang et al. [184] for LiB cells who tested nickel-rich layered oxides LiNi_{1-x-y}Mn_xCo_yO₂ (NMC622 with $x = y = 0.2$, NMC811 with $x = y = 0.1$, NMC9/0.5/0.5 with $x = y = 0.05$) and LFP with graphite counter electrode brings some information for comparative purposes against NVPF-based SiB cells. Nickel-rich layered oxides inherently possess more energy density and oxygen release from these structures might induce increased safety concerns; however, NVPF can be compared to LFP technology since both cathode materials have enhanced structural stability and common phosphate

group. The experimental abuse test was performed in a sealed chamber equipped with pressure sensor in an inert atmosphere. The heating plate and the battery were placed side by side and TR was triggered by lateral heating. The temperature increased slowly and reached the critical temperature after which the battery temperature rose rapidly. The TR critical temperature obtained were 155 °C, 121 °C, 131 °C, and 145 °C for NMC622, NMC811, NMC9/0.5/0.5, and LFP respectively. The more the delay in the critical temperature, the more enhanced the battery safety is. However, this critical temperature mostly depends on the processes taking place at the negative electrode (SEI breakdown followed by solvent reduction in contact with charged material), and thus is not impacted by the positive electrode material. The corresponding maximum thermal runaway temperatures reached were 559 °C, 803 °C, 842 °C, and 361 °C, respectively, as shown in Figure 15. The lower the maximum temperature of the battery, the less harmful the overall battery state is. Considering the maximal temperature that can be reached during TR, the LFP-based chemistry can be considered safer than Ni-rich NMC-based materials. The maximum temperature that can be reached for NMC-based materials increases due to higher energy density of the cell and higher propensity to release oxygen. Bugryniec et al. [185] also compared the LFP cells against LCO chemistry under convection by overheating in an oven and found that LFP cells are more stable and show less severe thermal behavior than LCO cells. For a NVPF||HC-based cell, as shown in Figure 14, it seems that the critical temperature failure also occurs around 125 °C, suggesting that processes on graphite and HC have the same impact on TR triggering. However, the NVPF||HC cell reaches lower maximal temperature than the LFP||graphite cell (286 °C versus 361 °C from [180,183]) which might highlight its increased safety. Following this, the more interesting point of comparison would be the gases analysis during TR to compare the overall safety of the technology.

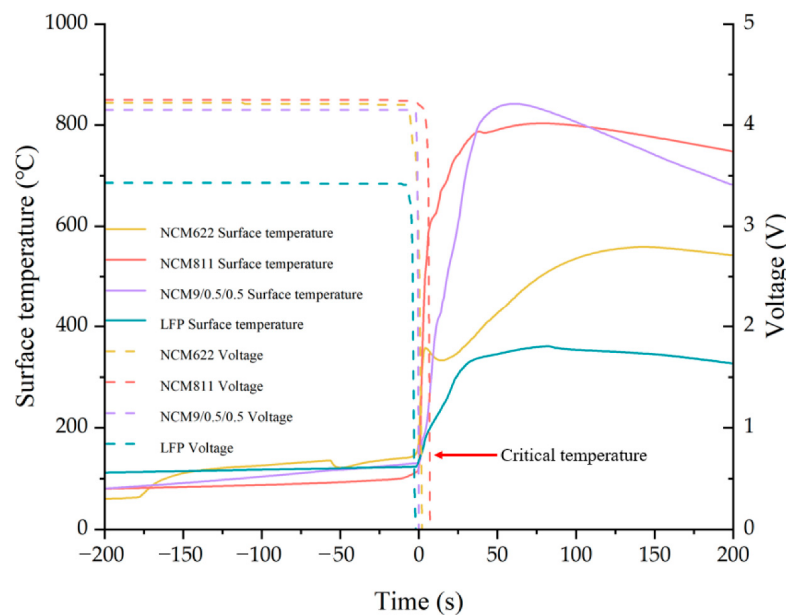


Figure 15. Battery sample surface temperature and voltage record changes. From reference [184] under CC BY 4.0.

Xie et al. [102] prepared sodium-pouch cell with layered oxide $\text{NaNi}_{1/3}\text{Fe}_{1/3}\text{Mn}_{1/3}\text{O}_2$ (NFM) cathode and HC anode and performed thermal runaway with Accelerating Rate Calorimetry (ARC). It was ramped at 5 K min^{-1} heating rate with heat-wait-seek protocol from 50 °C to approximately 300 °C [186]. Three distinct exothermal stages (Figure 16) were obtained; the first was at 166 °C, where SEI decomposition and the internal short-circuit might have taken place, the second at 243 °C, where battery temperature increased exponentially and reached $1\text{ }^{\circ}\text{C min}^{-1}$. The final temperature T3 was observed at 312 °C,

which was the peak maximal temperature. This temperature is significantly lower than that reached from most lithium-layered oxide cathode materials/graphite cells, as for instance around 800 °C for NMC111 or 803 °C for NMC811 cathodes, as discussed above [182,184]. These results serve as a proof of concept of the lower maximal temperature for a sodium-layered cathode during TR as compared to lithium-ion counterparts [187,188]. The overall general culmination behavior during thermal runaway is listed in Table 6.

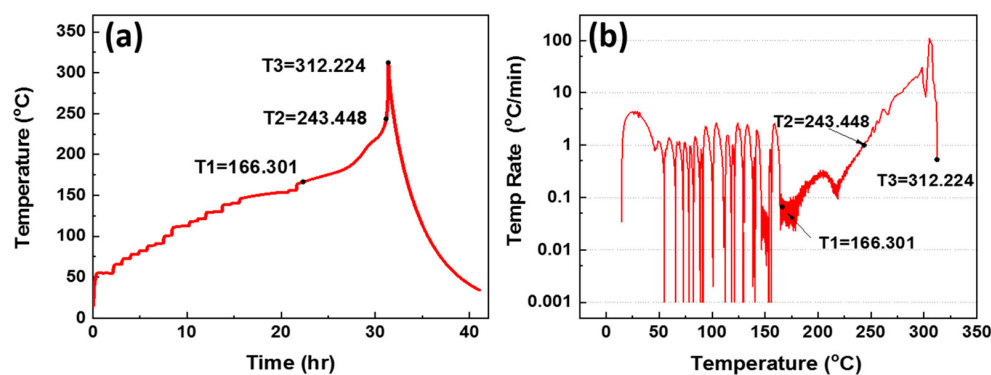


Figure 16. (a) Temperature vs. time, and (b) dT/dt vs. temperature plot of the charged NFM/HC cell under thermal stability testing with ARC. Reprinted with permission from [102]. Copyright 2018, American Chemical Society.

Table 6. Comparison between Li-ion and Na-ion T_{onset} and T_{max} reached during thermal runaway [102,181,184].

	Li-Ion			Na-Ion		
Phosphate-based materials	LFP	T_{onset} (°C)	T_{max} (°C)	NVPF	T_{onset} (°C)	T_{max} (°C)
Layered oxides	NMC622	155	559	NFM	125	286
	NMC811	121	803		166	312
	NMC9/0.5/0.5	131	842			

As potential alternative to non-graphitizable and disordered hard carbon structures, Li et al. [103] employed pyrolyzed anthracite (PA) anode obtained in the 1000–1400 °C temperature range in SiBs. PA have an anisotropic structure which resembles that of hard carbons between 1000 to 2000 °C with non-graphitizing carbons but can switch to high degree of graphitization above 2000 °C [189]. Pouch cells of O3-type layered oxide $\text{Na}_{0.9}[\text{Cu}_{0.22}\text{Fe}_{0.30}\text{Mn}_{0.48}]\text{O}_2$ as cathode and PA as anode exhibiting energy density of 100 Wh kg⁻¹ were fabricated. These pouch cells at 100% SOC were subjected to safety tests like external short circuit, overcharge and nail penetration tests, as shown in Figure 17. No smoke or fire were detected from these tests; however, the cells swelled at the end of the overcharge test maybe because of high voltages reached outside the electrochemical stability window of the electrolyte inducing its oxidation, leading to gas generation. However, the temperature increase was not of high magnitude for all safety tests. With the nail penetration test, the voltage returned to normal value once the nail was ejected from the system. These experiments also demonstrate the superior safety of SiBs system in these test conditions.

Hwang et al. [104] studied pouch cells composed of bare or Al_2O_3 coated O3-type $\text{Na}[\text{Ni}_{0.6}\text{Co}_{0.2}\text{Mn}_{0.2}]\text{O}_2$ layered oxide cathode and HC anode. The cells were tested in the voltage range of 1.0 to 4.1 V. Al_2O_3 -coated electrodes not only showed better coulombic efficiency but also showed an improvement in cycling performance. After charging, the cathode material was recovered from the current collector and DSC was performed at the scan rate of 5 °C min⁻¹ to assess the thermal stability. The desodiated bare $\text{Na}_{0.34}[\text{Ni}_{0.6}\text{Co}_{0.2}\text{Mn}_{0.2}]\text{O}_2$ shows an exothermic peak at 289 °C with heat generation of

753 J g⁻¹. These results were significantly improved with Al₂O₃ coated desodiated material showing better thermal stability with a smaller exothermic peak occurring at 295 °C and decreased heat generation of 625 J g⁻¹ as shown in Figure 18. The improved thermal stability was explained by uniform Al₂O₃ coating which prevents the oxidized cathode from being in direct contact with the electrolyte and delays oxygen release. These studies suggest that coating the active material is a good strategy not only to improve electrochemical performances but also overall cell safety.

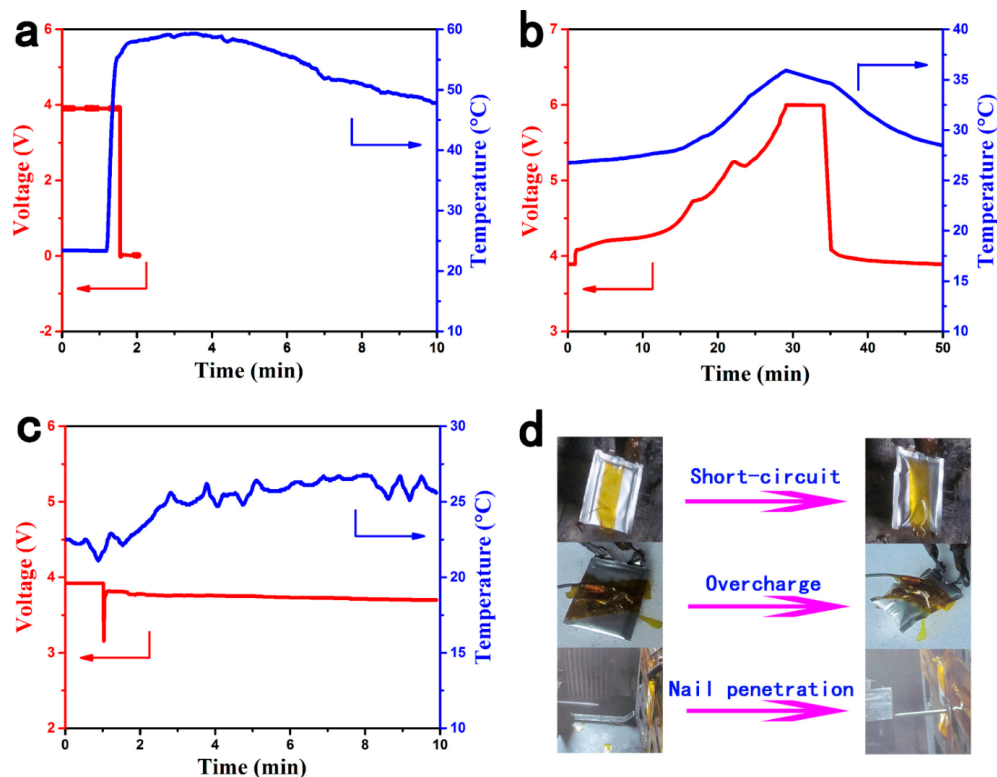


Figure 17. Voltage and temperature evolution process of (a) external short-circuit, (b) overcharge test, (c) nail penetration test, and (d) photographs of pouch cells before and after safety tests. Reproduced with permission from [103]. Copyright 2016, Elsevier.

However, the overall comparison of sodium-ion batteries to lithium-ion technology is intriguing. Based on the preliminary results obtained as detailed above, in general, sodium-ion batteries are more resilient to thermal runaway (lower T_{max} reached) and have less adverse thermal behavior and improved safety characteristics compared to lithium-ion batteries. However, sodium-based transition metal oxide cathodes have less structural stability (phase transitions) and higher moisture sensitivity than lithium-layered oxides [190,191]. Specificity of selected cathode chemistries must be considered while dealing with safety related issues. As shown in Table 3, typically, the extent of thermal runaway increases in the order of layered oxides > Prussian blue analogues > polyanionic materials. On the other hand, sodium salts are more thermally stable than lithium salts and can withstand more thermal stress than lithium-based salts. However, while dealing with thermal runaway, not only thermal threat but also chemical threat must be taken into consideration. As a matter of fact, fatalities from fires in enclosures generally result more and more from toxic smoke inhalation than from burns. Such fires involving batteries might not be an exception.

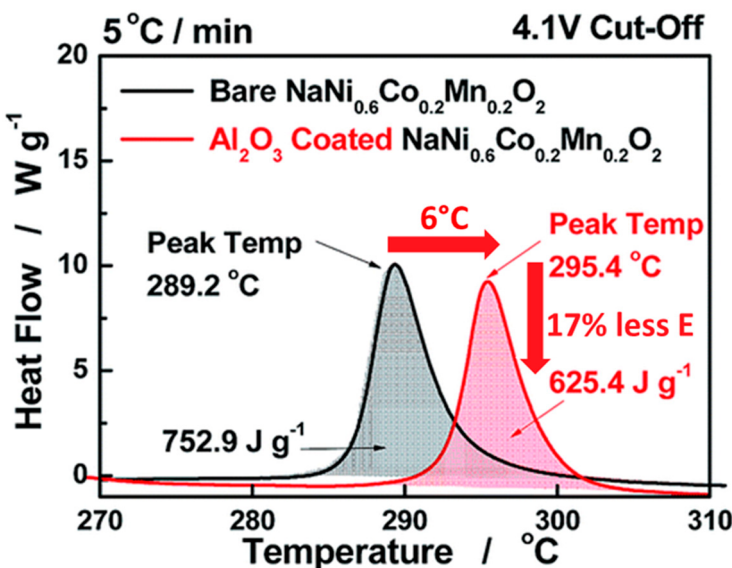


Figure 18. DSC data for uncoated and coated $\text{Na}[\text{Ni}_{0.6}\text{Co}_{0.2}\text{Mn}_{0.2}] \text{O}_2$ cathode. Reproduced with permission from [104]. Copyright 2017, Royal Society of Chemistry.

5. Role of the Separator in Battery Safety

The separator has a major contribution in battery safety preventing short circuits and malfunction as it lies in the middle of cathode and anode to prevent physical contact between the two electrodes [192–194]. It also facilitates sodium or lithium ions transport while blocking electron flow, and there exists a tradeoff between mechanical robustness for enhanced safety and ion transport properties [195]. The collapse of the separator by melting, shrinking, or vaporizing under high temperature leads to thermal runaway [196]. During cell abuse, the mechanical collision might cause mismatch in separator alignment leading to contact with electroactive species or during overcharge the metal dendrites might penetrate the separator leading to short-circuit. Hence, the separator must have high heat resistance for battery application at elevated temperature, good mechanical properties to withstand resistance against unfortunate calamities, be inert in the electrochemical stability range to suppress side reactions, and have high wettability compatibility with electrolytes to ensure effective ion migration and decrease in internal resistance [197].

Zhou et al. [196] fabricated NMC532 and graphite Li-ion pouch cells with four different separators: cellulose-based, trilayer PP/PE/PP, standard propylene, and homemade modified graphene-polydopamine coated separator. The latter is made of a PP separator soaked in polydopamine solution followed by slurry coating of carboxymethyl cellulose and graphene nanoflakes. The electrochemical formation cycles were conducted to form a uniform SEI layer, then the fully charged cells were subjected to ARC by employing the heat-wait-seek method. The in-house made separator showed the most improved thermal stability over the three commercial separators as evident from ARC experiment. This is suspected due to the enhanced mechanical robustness and anti-shrinkage properties under abusive conditions, such approaches using modified separators must be applied to SiB or LiB technology to maximize safety. Zu et al. [198] developed polyolefin-based separators with reactive $\text{Mg}(\text{OH})_2@\text{MgO}$ coatings to tackle lithium metal dendrite formation on lithium metal anode when cycled in liquid electrolyte. This protective coating interacts with lithium metal to eliminate lithium protuberance and facilitate uniform metal deposition. Such an approach can be extended to LiB and emerging SiB technologies to eliminate alkali metal dendritic plating while cycling at high current rates or low temperature, and thus ensure added safety.

Conventional polyolefin (polyethylene or polypropylene) separators have poor wetting with SiB liquid electrolyte and low ionic conductivity in NaPF_6^- - and NaClO_4 -based sodium salts [199,200]. Ho et al. [199] introduced a poly(dopamine) modified PE separator

by dip coating method; the dopamine incorporation in the PE separator increased the hydrophilicity of PE separator and promoted ionic conductivity. As a result, the electrochemical performance in HC half cells was improved as compared to a bare PE separator. Kim et al. [200] demonstrated that an SiO_2 thin layer coated with Chemical Vapor Deposition (CVD) method onto a PE separator improved wettability with the electrolyte and ion transport properties. Therefore, the development of innovative coatings on polyolefin separators seems a great strategy to boost battery safety owing to the possibility of lowering internal resistance through wettability enhancement and avoiding short-circuits through elimination of alkali dendrite formation at the anode upon cycling and separator shrinkage upon thermal event.

6. Conclusions and Perspectives

Battery researchers often deal with the development and further improvement of high-energy or high-power cells with good cyclability. However, too often yet, the safety of the battery is not part of the primary focus. As frequent battery failures with large thermal runaways may cost hundreds of lives, battery safety must be accessed with equal priority. In this regard, this paper discusses the current understanding of safety issues pertaining to the emerging sodium-ion batteries. They possess advantages like reduced cost of production due to high sodium abundance, a similar working principle, and the possibility of using cheaper and lighter aluminum current collectors. The latter favors the over-discharge phenomenon, promoting zero-volt storage and safer handling and shipping. Even though LiBs and SiBs function with a similar charge–discharge phenomenon, the same pre-established set of rules with analogous corresponding cathode or electrolyte will not function prominently. It is a system that needs to be optimized differently to maintain stable interfaces with electrolyte engineering. Indeed, the SEI in SiBs is generally reported to be more vulnerable than in LiBs. Here, we talk about how the electrolyte optimization aids to mitigate this issue and delay SEI breakdown at the origin of the thermal runaway triggering. As with LiBs, identifying additives with a synergistic effect that is truly exceptional remains a significant challenge. This paper also compares most of the electrode materials commonly used in SiBs and LiBs. The studied desodiated layered oxides showed better thermal stability. However, further layered oxide materials and proofs of the exothermic thermal decomposition paths in presence or not of the electrolyte still require in-depth investigations to generalize on the better thermal stability of this cathode family. These studies can benefit from the latest cutting-edge operando technologies. As example, real-time in situ TEM studies taught a lesson to find an optimum between cycling to higher voltages to extract the maximum capacity and maintaining the cathode structure upon heating, focusing on safety. However, some sodium-ion cells, NVPF||HC or O₃-type layered oxide $\text{Na}_{0.9}[\text{Cu}_{0.22}\text{Fe}_{0.30}\text{Mn}_{0.48}]\text{O}_2$ ||pyrolyzed anthracite, showed no flaming combustion during thermal abuse tests or when exposed to external short circuits, overcharge tests, or nail penetration tests, respectively, encouraging companies like Tiamat, CATL, Altris AB, or Faradion to turn the pages of proposed future SiBs from research papers to the physical batteries of today. With great inventions come even greater responsibilities; hence, one must access great depths into the safety of such latest technologies. As in the case of Li-ion, Na-ion is not based on one unique chemistry, and therefore any new variant of Na-ion needs to be reassessed and relating safety profile must be examined. Furthermore, its threats should be benchmarked with potential alternatives before any choice for a given application.

Author Contributions: Conceptualization, G.M.; Validation, S.G., A.E.M., S.L. and G.M.; Investigation, P.T.B.; Writing—Original Draft Preparation, P.T.B.; Writing—Review and Editing, S.G. and G.M.; Visualization, P.T.B.; Resources, A.E.M.; Supervision, S.L. and G.M.; Project Administration, S.L. and G.M. All authors have read and agreed to the published version of the manuscript.

Funding: As a part of the DESTINY Ph.D. program, this publication is acknowledged by funding from the European Union's Horizon2020 research and innovation program under the Marie Skłodowska-Curie Actions COFUND (Grant Agreement #945357).

Data Availability Statement: No new data were created in this study. Data sharing is not applicable to this article.

Conflicts of Interest: Author Asmae El Mejdoubi was employed by the company TIAMAT. The remaining authors declare that the research was conducted in the absence of any commercial or financial relationships that could be construed as a potential conflict of interest.

References

1. Luo, X.; Wang, J.; Dooner, M.; Clarke, J. Overview of Current Development in Electrical Energy Storage Technologies and the Application Potential in Power System Operation. *Appl. Energy* **2015**, *137*, 511–536. [CrossRef]
2. Mitali, J.; Dhinakaran, S.; Mohamad, A.A. Energy Storage Systems: A Review. *Energy Storage Sav.* **2022**, *1*, 166–216. [CrossRef]
3. Kurzweil, P. Gaston Planté and His Invention of the Lead–Acid Battery—The Genesis of the First Practical Rechargeable Battery. *J. Power Sources* **2010**, *195*, 4424–4434. [CrossRef]
4. Zhu, X.; Li, L.; Sun, X.; Yang, D.; Gao, L.; Liu, J.; Kumar, R.V.; Yang, J. Preparation of Basic Lead Oxide from Spent Lead Acid Battery Paste via Chemical Conversion. *Hydrometallurgy* **2012**, *117*–*118*, 24–31. [CrossRef]
5. Fire Hazard Assessment of Lead-Acid Batteries. Available online: <https://www.nfpa.org/education-and-research/research/fire-protection-research-foundation/projects-and-reports/fire-hazard-assessment-of-lead-acid-batteries> (accessed on 3 October 2024).
6. Zhang, J.; Chen, C.; Zhang, X.; Liu, S. Study on the Environmental Risk Assessment of Lead-Acid Batteries. *Procedia Environ. Sci.* **2016**, *31*, 873–879. [CrossRef]
7. World Health Organization. Recycling Used Lead-Acid Batteries: Health Considerations. World Health Organization: Geneva, Switzerland, 2017; ISBN 978-92-4-151285-5. Available online: <https://iris.who.int/handle/10665/259447> (accessed on 3 October 2024).
8. Bernard, P. Secondary Batteries—Nickel Systems | Nickel–Cadmium: Sealed. In *Encyclopedia of Electrochemical Power Sources*; Elsevier: Amsterdam, The Netherlands, 2009; pp. 459–481, ISBN 978-0-444-52745-5. Available online: <https://linkinghub.elsevier.com/retrieve/pii/b9780444527455001544> (accessed on 3 October 2024).
9. EU Bans Nickel–Cadmium Batteries in Portable Devices by 2025: Impact on Emergency Lighting. Available online: <https://www.etaplighting.com/en/blog/end-of-cadmium-batteries-portable-applications> (accessed on 16 April 2024).
10. Maxianova, K.; Rusche, T.M. Restriction of Hazardous Substances: On the Need for and the Limits of Comitology. *Rev. Eur. Community Int. Environ. Law* **2006**, *15*, 202–210. [CrossRef]
11. Bernard, P.; Lippert, M. Nickel–Cadmium and Nickel–Metal Hydride Battery Energy Storage. In *Electrochemical Energy Storage for Renewable Sources and Grid Balancing*; Elsevier: Amsterdam, The Netherlands, 2015; pp. 223–251, ISBN 978-0-444-62616-5. Available online: <https://linkinghub.elsevier.com/retrieve/pii/b9780444626165000140> (accessed on 3 October 2024).
12. Ikoma, M.; Yuasa, S.; Yuasa, K.; Kaida, S.; Matsumoto, I.; Iwakura, C. Charge Characteristics of Sealed-Type Nickel/Metal-Hydride Battery. *J. Alloys Compd.* **1998**, *267*, 252–256. [CrossRef]
13. Winn, D.A.; Shemilt, J.M.; Steele, B.C.H. Titanium Disulphide: A Solid Solution Electrode for Sodium and Lithium. *Mater. Res. Bull.* **1976**, *11*, 559–566. [CrossRef]
14. Whittingham, M.S. Electrical Energy Storage and Intercalation Chemistry. *Science* **1976**, *192*, 1126–1127. [CrossRef]
15. Cairns, E.J.; Shimotake, H. High-Temperature Batteries: Research in High-Temperature Electrochemistry Reveals Compact, Powerful Energy-Storage Cells. *Science* **1969**, *164*, 1347–1355. [CrossRef]
16. Nishi, Y. Lithium Ion Secondary Batteries; Past 10 Years and the Future. *J. Power Sources* **2001**, *100*, 101–106. [CrossRef]
17. Feng, X.; Ouyang, M.; Liu, X.; Lu, L.; Xia, Y.; He, X. Thermal Runaway Mechanism of Lithium Ion Battery for Electric Vehicles: A Review. *Energy Storage Mater.* **2018**, *10*, 246–267. [CrossRef]
18. Forestier, C.; Gruegon, S.; Davoisne, C.; Lecocq, A.; Marlair, G.; Armand, M.; Sannier, L.; Laruelle, S. Graphite Electrode Thermal Behavior and Solid Electrolyte Interphase Investigations: Role of State-of-the-Art Binders, Carbonate Additives and Lithium Bis(Fluorosulfonyl)Imide Salt. *J. Power Sources* **2016**, *330*, 186–194. [CrossRef]
19. Kim, G.-H.; Pesaran, A.; Spotnitz, R. A Three-Dimensional Thermal Abuse Model for Lithium-Ion Cells. *J. Power Sources* **2007**, *170*, 476–489. [CrossRef]
20. Spotnitz, R.; Franklin, J. Abuse Behavior of High-Power, Lithium-Ion Cells. *J. Power Sources* **2003**, *113*, 81–100. [CrossRef]
21. Nie, B.; Dong, Y.; Chang, L. The Evolution of Thermal Runaway Parameters of Lithium-Ion Batteries under Different Abuse Conditions: A Review. *J. Energy Storage* **2024**, *96*, 112624. [CrossRef]
22. Tobishima, S.; Yamaki, J. A Consideration of Lithium Cell Safety. *J. Power Sources* **1999**, *81*–*82*, 882–886. [CrossRef]
23. Tobishima, S.; Takei, K.; Sakurai, Y.; Yamaki, J. Lithium Ion Cell Safety. *J. Power Sources* **2000**, *90*, 188–195. [CrossRef]
24. Kitoh, K.; Nemoto, H. 100 Wh Large Size Li-Ion Batteries and Safety Tests. *J. Power Sources* **1999**, *81*–*82*, 887–890. [CrossRef]
25. Lyu, Y.; Wu, X.; Wang, K.; Feng, Z.; Cheng, T.; Liu, Y.; Wang, M.; Chen, R.; Xu, L.; Zhou, J.; et al. An Overview on the Advances of LiCoO₂ Cathodes for Lithium-Ion Batteries. *Adv. Energy Mater.* **2021**, *11*, 2000982. [CrossRef]
26. Cho, J.; Kim, Y.J.; Park, B. Novel LiCoO₂ Cathode Material with Al₂O₃ Coating for a Li Ion Cell. *Chem. Mater.* **2000**, *12*, 3788–3791. [CrossRef]

27. Jo, M.; Hong, Y.-S.; Choo, J.; Cho, J. Effect of LiCoO₂ Cathode Nanoparticle Size on High Rate Performance for Li-Ion Batteries. *J. Electrochem. Soc.* **2009**, *156*, A430. [[CrossRef](#)]
28. Ahangari, M.; Szalai, B.; Lujan, J.; Zhou, M.; Luo, H. Advancements and Challenges in High-Capacity Ni-Rich Cathode Materials for Lithium-Ion Batteries. *Materials* **2024**, *17*, 801. [[CrossRef](#)]
29. Xia, Y.; Zheng, J.; Wang, C.; Gu, M. Designing Principle for Ni-Rich Cathode Materials with High Energy Density for Practical Applications. *Nano Energy* **2018**, *49*, 434–452. [[CrossRef](#)]
30. Zhang, S.S. Problems and Their Origins of Ni-Rich Layered Oxide Cathode Materials. *Energy Storage Mater.* **2020**, *24*, 247–254. [[CrossRef](#)]
31. Chakraborty, A.; Kunnikuruvan, S.; Kumar, S.; Markovsky, B.; Aurbach, D.; Dixit, M.; Major, D.T. Layered Cathode Materials for Lithium-Ion Batteries: Review of Computational Studies on LiNi_{1-x-y}Co_xMn_yO₂ and LiNi_{1-x-y}Co_xAl_yO₂. *Chem. Mater.* **2020**, *32*, 915–952. [[CrossRef](#)]
32. Vitins, G.; West, K. Lithium Intercalation into Layered LiMnO₂. *J. Electrochem. Soc.* **1997**, *144*, 2587–2592. [[CrossRef](#)]
33. Berg, H.; Göransson, K.; Noläng, B.; Thomas, J.O. Electronic Structure and Stability of the Li_xMn₂O₄ (0 < x < 2) System. *J. Mater. Chem.* **1999**, *9*, 2813–2820. [[CrossRef](#)]
34. Cheruku, R.; Kruthika, G.; Govindaraj, G.; Vijayan, L. Electrical Relaxation Studies of Olivine Type Nanocrystalline LiMPO₄ (M=Ni, Mn and Co) Materials. *J. Phys. Chem. Solids* **2015**, *86*, 27–35. [[CrossRef](#)]
35. Manthiram, A. A Reflection on Lithium-Ion Battery Cathode Chemistry. *Nat. Commun.* **2020**, *11*, 1550. [[CrossRef](#)]
36. Benoit, C.; Franger, S. Chemistry and Electrochemistry of Lithium Iron Phosphate. *J. Solid. State Electrochem.* **2008**, *12*, 987–993. [[CrossRef](#)]
37. Dahn, J.; Fuller, E.; Obrovac, M.; Vonsacken, U. Thermal Stability of Li_xCoO₂, Li_xNiO₂ and λ-MnO₂ and Consequences for the Safety of Li-Ion Cells. *Solid. State Ion.* **1994**, *69*, 265–270. [[CrossRef](#)]
38. Bak, S.-M.; Hu, E.; Zhou, Y.; Yu, X.; Senanayake, S.D.; Cho, S.-J.; Kim, K.-B.; Chung, K.Y.; Yang, X.-Q.; Nam, K.-W. Structural Changes and Thermal Stability of Charged LiNi_xMn_yCo_zO₂ Cathode Materials Studied by Combined In Situ Time-Resolved XRD and Mass Spectroscopy. *ACS Appl. Mater. Interfaces* **2014**, *6*, 22594–22601. [[CrossRef](#)]
39. Rumble, C.; Conry, T.E.; Doeff, M.; Cairns, E.J.; Penner-Hahn, J.E.; Deb, A. Structural and Electrochemical Investigation of Li(Ni_{0.4}Co_{0.15}Al_{0.05}Mn_{0.4})O₂ Cathode Material. *J. Electrochem. Soc.* **2010**, *157*, A1317. [[CrossRef](#)]
40. Wang, J.; Li, Y.; Liu, R.; Xu, X.-M.; Zeng, C.-S.; Shen, X.-B.; Gu, Y.-J. The Different Roles of Ni²⁺/Ni³⁺, Ni³⁺/Ni⁴⁺, and Mn³⁺/Mn⁴⁺ in Li-Rich Layered Nanostructured LiNi_{1-x}Mn_xO₂·Li₂MnO₃ with High Capacity. *Int. J. Electrochem. Sci.* **2021**, *16*, 210425. [[CrossRef](#)]
41. Schafzahl, L.; Mahne, N.; Schafzahl, B.; Wilkening, M.; Slugovc, C.; Borisov, S.M.; Freunberger, S.A. Singlet Oxygen during Cycling of the Aprotic Sodium-O₂ Battery. *Angew. Chem. Int. Ed. Engl.* **2017**, *56*, 15728–15732. [[CrossRef](#)]
42. Kalyani, P.; Kalaiselvi, N. Various Aspects of LiNiO₂ Chemistry: A Review. *Sci. Technol. Adv. Mater.* **2005**, *6*, 689–703. [[CrossRef](#)]
43. Salomez, B.; Grugue, S.; Armand, M.; Tran-Van, P.; Laruelle, S. Review—Gassing Mechanisms in Lithium-Ion Battery. *J. Electrochem. Soc.* **2023**, *170*, 050537. [[CrossRef](#)]
44. Kebede, M.A.; Ezema, F.I. (Eds.) *Electrochemical Devices for Energy Storage Applications*, 1st ed.; CRC Press: Boca Raton, FL, USA, 2019; ISBN 978-0-367-85511-6. Available online: <https://www.taylorfrancis.com/books/9781000763799> (accessed on 3 October 2024).
45. Mao, N.; Gadkari, S.; Wang, Z.; Zhang, T.; Bai, J.; Cai, Q. A Comparative Analysis of Lithium-Ion Batteries with Different Cathodes under Overheating and Nail Penetration Conditions. *Energy* **2023**, *278*, 128027. [[CrossRef](#)]
46. Brand, M.; Gläser, S.; Geder, J.; Menacher, S.; Obpacher, S.; Jossen, A.; Quinger, D. Electrical Safety of Commercial Li-Ion Cells Based on NMC and NCA Technology Compared to LFP Technology. *World Electr. Veh. J.* **2013**, *6*, 572–580. [[CrossRef](#)]
47. Bugryniec, P.J.; Resendiz, E.G.; Nwophoke, S.M.; Khanna, S.; James, C.; Brown, S.F. Review of Gas Emissions from Lithium-Ion Battery Thermal Runaway Failure—Considering Toxic and Flammable Compounds. *J. Energy Storage* **2024**, *87*, 111288. [[CrossRef](#)]
48. Azuma, H.; Imoto, H.; Yamada, S.; Sekai, K. Advanced Carbon Anode Materials for Lithium Ion Cells. *J. Power Sources* **1999**, *81–82*, 1–7. [[CrossRef](#)]
49. Asenbauer, J.; Eisenmann, T.; Kuenzel, M.; Kazzazi, A.; Chen, Z.; Bresser, D. The Success Story of Graphite as a Lithium-Ion Anode Material—Fundamentals, Remaining Challenges, and Recent Developments Including Silicon (Oxide) Composites. *Sustain. Energy Fuels* **2020**, *4*, 5387–5416. [[CrossRef](#)]
50. Li, L.; Zhang, D.; Deng, J.; Gou, Y.; Fang, J.; Cui, H.; Zhao, Y.; Cao, M. Carbon-Based Materials for Fast Charging Lithium-Ion Batteries. *Carbon* **2021**, *183*, 721–734. [[CrossRef](#)]
51. Yoon, T.; Milien, M.S.; Parimalam, B.S.; Lucht, B.L. Thermal Decomposition of the Solid Electrolyte Interphase (SEI) on Silicon Electrodes for Lithium Ion Batteries. *Chem. Mater.* **2017**, *29*, 3237–3245. [[CrossRef](#)]
52. Sick, N.; Krätzig, O.; Eshetu, G.G.; Figgemeier, E. A Review of the Publication and Patent Landscape of Anode Materials for Lithium Ion Batteries. *J. Energy Storage* **2021**, *43*, 103231. [[CrossRef](#)]
53. Yan, H.; Zhang, D.; Qilu; Duo, X.; Sheng, X. A Review of Spinel Lithium Titanate (Li₄Ti₅O₁₂) as Electrode Material for Advanced Energy Storage Devices. *Ceram. Int.* **2021**, *47*, 5870–5895. [[CrossRef](#)]
54. Belharouak, I.; Koenig, G.M.; Amine, K. Electrochemistry and Safety of Li₄Ti₅O₁₂ and Graphite Anodes Paired with LiMn₂O₄ for Hybrid Electric Vehicle Li-Ion Battery Applications. *J. Power Sources* **2011**, *196*, 10344–10350. [[CrossRef](#)]
55. Abraham, K.M. How Comparable Are Sodium-Ion Batteries to Lithium-Ion Counterparts? *ACS Energy Lett.* **2020**, *5*, 3544–3547. [[CrossRef](#)]

56. PV magazine International Sodium-Ion Batteries—A Viable Alternative to Lithium? Available online: <https://www.pv-magazine.com/2024/03/22/sodium-ion-batteries-a-viable-alternative-to-lithium/> (accessed on 23 September 2024).
57. Lithium ion Battery Manufacturer and Supplier in China-DNK Power Will Sodium Batteries Replace Lithium Batteries? Available online: <https://www.dnkpower.com/will-sodium-batteries-replace-lithium-batteries/> (accessed on 23 September 2024).
58. Desai, P.; Forero-Saboya, J.; Meunier, V.; Rousse, G.; Deschamps, M.; Abakumov, A.M.; Tarascon, J.-M.; Mariyappan, S. Mastering the Synergy between Na₃V₂(PO₄)₂F₃ Electrode and Electrolyte: A Must for Na-Ion Cells. *Energy Storage Mater.* **2023**, *57*, 102–117. [CrossRef]
59. Tournevis Sans Fil DEXTER Sodium 3.6 V 0.7 Ah | Leroy Merlin. Available online: <https://www.leroymerlin.fr/produits/outillage/outillage-electroportatif/visseuse-et-tournevis-electrique/visseuse/tournevis-sans-fil-dexter-sodium-3-6-v-0-7-ah-86650845.html> (accessed on 8 July 2024).
60. Barker, J.; Heap, R.J.; Roche, N.; Tan, C.; Sayers, R.; Whitley, J.; Liu, Y. High Energy Density Na-Ion Battery Technology. *Meet. Abstr.* **2016**, *MA2016-03*, 796. [CrossRef]
61. Faradion Transport Applications. Available online: <https://faradion.co.uk/applications/transport-applications/> (accessed on 14 June 2023).
62. Gupta, Y.; Siwatch, P.; Karwasra, R.; Sharma, K.; Tripathi, S.K. Recent Progress of Layered Structured P₂- and O₃-Type Transition Metal Oxides as Cathode Material for Sodium-Ion Batteries. *Renew. Sustain. Energy Rev.* **2024**, *192*, 114167. [CrossRef]
63. Wang, P.-F.; You, Y.; Yin, Y.-X.; Guo, Y.-G. Layered Oxide Cathodes for Sodium-Ion Batteries: Phase Transition, Air Stability, and Performance. *Adv. Energy Mater.* **2018**, *8*, 1701912. [CrossRef]
64. Grépin, E.; Jacquet, Q.; Moiseev, I.A.; Iadecola, A.; Rousse, G.; Avdeev, M.; Abakumov, A.M.; Tarascon, J.-M.; Mariyappan, S. Mastering the Synthesis of High Na-Content, Moisture-Stable Layered Oxide Cathode for Na-Ion Batteries. *J. Power Sources* **2024**, *613*, 234962. [CrossRef]
65. Huang, Y.; Zeng, W.; Li, K.; Zhu, X. Na-Deficient P₂-Type Layered Oxide Cathodes for Practical Sodium-Ion Batteries. *Microstructures* **2024**, *4*, 2024027. [CrossRef]
66. Ni, Q.; Bai, Y.; Wu, F.; Wu, C. Polyanion-Type Electrode Materials for Sodium-Ion Batteries. *Adv. Sci.* **2017**, *4*, 1600275. [CrossRef]
67. Xu, C.; Zhao, J.; Yang, C.; Hu, Y.-S. Polyanionic Cathode Materials for Practical Na-Ion Batteries toward High Energy Density and Long Cycle Life. *ACS Cent. Sci.* **2023**, *9*, 1721–1736. [CrossRef]
68. Li, H.; Xu, M.; Zhang, Z.; Lai, Y.; Ma, J. Engineering of Polyanion Type Cathode Materials for Sodium-Ion Batteries: Toward Higher Energy/Power Density. *Adv. Funct. Mater.* **2020**, *30*, 2000473. [CrossRef]
69. Lv, Z.; Ling, M.; Yue, M.; Li, X.; Song, M.; Zheng, Q.; Zhang, H. Vanadium-Based Polyanionic Compounds as Cathode Materials for Sodium-Ion Batteries: Toward High-Energy and High-Power Applications. *J. Energy Chem.* **2021**, *55*, 361–390. [CrossRef]
70. He, M.; Davis, R.; Chartouni, D.; Johnson, M.; Abplanalp, M.; Troendle, P.; Sutterlin, R.-P. Assessment of the First Commercial Prussian Blue Based Sodium-Ion Battery. *J. Power Sources* **2022**, *548*, 232036. [CrossRef]
71. Sodium-Ion Batteries & Sustainable Energy | Natron Energy. Available online: <https://natron.energy/> (accessed on 8 July 2024).
72. Bie, X.; Kubota, K.; Hosaka, T.; Chihara, K.; Komaba, S. Synthesis and Electrochemical Properties of Na-Rich Prussian Blue Analogues Containing Mn, Fe, Co, and Fe for Na-Ion Batteries. *J. Power Sources* **2018**, *378*, 322–330. [CrossRef]
73. Han, J.; Lin, Y.; Yang, Y.; Zuo, D.; Wang, C.; Liu, X. Dominant Role of M Element on the Stability and Properties of Prussian Blue Analogues NaxMFe(CN)₆ (M = 3d Transition Metal) as Cathode Material for the Sodium-Ion Batteries. *J. Alloys Compd.* **2021**, *870*, 159533. [CrossRef]
74. Ojwang, D.O.; Häggström, L.; Ericsson, T.; Ångström, J.; Brant, W.R. Influence of Sodium Content on the Thermal Behavior of Low Vacancy Prussian White Cathode Material. *Dalton Trans.* **2020**, *49*, 3570–3579. [CrossRef]
75. Xiao, Y.; Xiao, J.; Zhao, H.; Li, J.; Zhang, G.; Zhang, D.; Guo, X.; Gao, H.; Wang, Y.; Chen, J.; et al. Prussian Blue Analogues for Sodium-Ion Battery Cathodes: A Review of Mechanistic Insights, Current Challenges, and Future Pathways. *Small* **2024**, *2401957*. [CrossRef]
76. Perveen, T.; Siddiq, M.; Shahzad, N.; Ihsan, R.; Ahmad, A.; Shahzad, M.I. Prospects in Anode Materials for Sodium Ion Batteries—A Review. *Renew. Sustain. Energy Rev.* **2020**, *119*, 109549. [CrossRef]
77. Wang, H.; Chen, S.; Fu, C.; Ding, Y.; Liu, G.; Cao, Y.; Chen, Z. Recent Advances in Conversion-Type Electrode Materials for Post Lithium-Ion Batteries. *ACS Mater. Lett.* **2021**, *3*, 956–977. [CrossRef]
78. Lübke, M.; Howard, D.; Armer, C.F.; Gardecka, A.J.; Lowe, A.; Reddy, M.V.; Liu, Z.; Darr, J.A. High Energy Lithium Ion Battery Electrode Materials; Enhanced Charge Storage via Both Alloying and Insertion Processes. *Electrochim. Acta* **2017**, *231*, 247–254. [CrossRef]
79. Moriwake, H.; Kuwabara, A.; Fisher, C.A.J.; Ikuhara, Y. Why Is Sodium-Intercalated Graphite Unstable? *RSC Adv.* **2017**, *7*, 36550–36554. [CrossRef]
80. Dou, X.; Hasa, I.; Saurel, D.; Vaalma, C.; Wu, L.; Buchholz, D.; Bresser, D.; Komaba, S.; Passerini, S. Hard Carbons for Sodium-Ion Batteries: Structure, Analysis, Sustainability, and Electrochemistry. *Mater. Today* **2019**, *23*, 87–104. [CrossRef]
81. Nayak, P.K.; Yang, L.; Brehm, W.; Adelhelm, P. From Lithium-Ion to Sodium-Ion Batteries: Advantages, Challenges, and Surprises. *Angew. Chem. Int. Ed.* **2018**, *57*, 102–120. [CrossRef]
82. Hwang, J.-Y.; Myung, S.-T.; Sun, Y.-K. Sodium-Ion Batteries: Present and Future. *Chem. Soc. Rev.* **2017**, *46*, 3529–3614. [CrossRef]

83. Zhang, H.; Gao, Y.; Liu, X.; Yang, Z.; He, X.; Li, L.; Qiao, Y.; Chen, W.; Zeng, R.; Wang, Y.; et al. Organic Cathode Materials for Sodium-Ion Batteries: From Fundamental Research to Potential Commercial Application. *Adv. Funct. Mater.* **2022**, *32*, 2107718. [[CrossRef](#)]
84. Xu, Y.; Zhou, M.; Lei, Y. Organic Materials for Rechargeable Sodium-Ion Batteries. *Mater. Today* **2018**, *21*, 60–78. [[CrossRef](#)]
85. Stevens, D.A.; Dahn, J.R. High Capacity Anode Materials for Rechargeable Sodium-Ion Batteries. *J. Electrochem. Soc.* **2000**, *147*, 1271. [[CrossRef](#)]
86. Sun, Y.-F.; Li, Y.; Gong, Y.-T.; Qiu, Z.-X.; Qian, J.; Bai, Y.; Wang, Z.-L.; Zhang, R.-P.; Wu, C. Constructing Three-Dimensional Architectures to Design Advanced Anodes Materials for Sodium-Ion Batteries: From Nanoscale to Microscale. *Energy Mater.* **2024**, *4*, 400002. [[CrossRef](#)]
87. Song, B.; Li, W.; Oh, S.-M.; Manthiram, A. Long-Life Nickel-Rich Layered Oxide Cathodes with a Uniform Li_2ZrO_3 Surface Coating for Lithium-Ion Batteries. *ACS Appl. Mater. Interfaces* **2017**, *9*, 9718–9725. [[CrossRef](#)]
88. Liu, S.; Liu, Z.; Shen, X.; Li, W.; Gao, Y.; Banis, M.N.; Li, M.; Chen, K.; Zhu, L.; Yu, R.; et al. Surface Doping to Enhance Structural Integrity and Performance of Li-Rich Layered Oxide. *Adv. Energy Mater.* **2018**, *8*, 1802105. [[CrossRef](#)]
89. Eshetu, G.G.; Grugeon, S.; Gachot, G.; Mathiron, D.; Armand, M.; Laruelle, S. LiFSI vs. LiPF6 Electrolytes in Contact with Lithiated Graphite: Comparing Thermal Stabilities and Identification of Specific SEI-Reinforcing Additives. *Electrochim. Acta* **2013**, *102*, 133–141. [[CrossRef](#)]
90. Eshetu, G.G.; Diemant, T.; Hekmatfar, M.; Grugeon, S.; Behm, R.J.; Laruelle, S.; Armand, M.; Passerini, S. Impact of the Electrolyte Salt Anion on the Solid Electrolyte Interphase Formation in Sodium Ion Batteries. *Nano Energy* **2019**, *55*, 327–340. [[CrossRef](#)]
91. Liu, Q.; Su, X.; Lei, D.; Qin, Y.; Wen, J.; Guo, F.; Wu, Y.A.; Rong, Y.; Kou, R.; Xiao, X.; et al. Approaching the Capacity Limit of Lithium Cobalt Oxide in Lithium Ion Batteries via Lanthanum and Aluminium Doping. *Nat. Energy* **2018**, *3*, 936–943. [[CrossRef](#)]
92. Välikangas, J.; Laine, P.; Hietaniemi, M.; Hu, T.; Tynjälä, P.; Lassi, U. Precipitation and Calcination of High-Capacity LiNiO_2 Cathode Material for Lithium-Ion Batteries. *Appl. Sci.* **2020**, *10*, 8988. [[CrossRef](#)]
93. Myung, S.-T.; Komaba, S.; Kumagai, N. Orthorhombic LiMnO_2 as a High Capacity Cathode for Lithium-Ion Battery Synthesized by Hydrothermal Route at 170 °C. *Chem. Lett.* **2001**, *30*, 80–81. [[CrossRef](#)]
94. Wagner, A.C.; Bohn, N.; Geßwein, H.; Neumann, M.; Osenberg, M.; Hilger, A.; Manke, I.; Schmidt, V.; Binder, J.R. Hierarchical Structuring of NMC111-Cathode Materials in Lithium-Ion Batteries: An In-Depth Study on the Influence of Primary and Secondary Particle Sizes on Electrochemical Performance. *ACS Appl. Energy Mater.* **2020**, *3*, 12565–12574. [[CrossRef](#)]
95. Tadesse, P.; Gebrekirnos, H.; Semu, G.; Duressa, M.; Chemedya, Y.C.; Murali, N.; Babu, K.V. Investigation of Structural, Vibrational Spectroscopic and Properties Study of LiMn_2O_4 and $\text{LiMn}_{1.9}\text{Cu}_{0.05}\text{Fe}_{0.05}\text{O}_4$ Cathode Materials. *Results Mater.* **2021**, *12*, 100224. [[CrossRef](#)]
96. Li, H.; Peng, L.; Wu, D.; Wu, J.; Zhu, Y.; Hu, X. Ultrahigh-Capacity and Fire-Resistant LiFePO_4 -Based Composite Cathodes for Advanced Lithium-Ion Batteries. *Adv. Energy Mater.* **2019**, *9*, 1802930. [[CrossRef](#)]
97. Zhao, J.; Zhao, L.; Dimov, N.; Okada, S.; Nishida, T. Electrochemical and Thermal Properties of $\alpha\text{-NaFeO}_2$ Cathode for Na-Ion Batteries. *J. Electrochem. Soc.* **2013**, *160*, A3077–A3081. [[CrossRef](#)]
98. Barpanda, P.; Liu, G.; Ling, C.D.; Tamaru, M.; Avdeev, M.; Chung, S.-C.; Yamada, Y.; Yamada, A. $\text{Na}_2\text{FeP}_2\text{O}_7$: A Safe Cathode for Rechargeable Sodium-Ion Batteries. *Chem. Mater.* **2013**, *25*, 3480–3487. [[CrossRef](#)]
99. Liu, Y.; Wu, Z.; Indris, S.; Hua, W.; Casati, N.P.M.; Tayal, A.; Darma, M.S.D.; Wang, G.; Liu, Y.; Wu, C.; et al. The Structural Origin of Enhanced Stability of $\text{Na}_{3.32}\text{Fe}_{2.11}\text{Ca}_{0.23}(\text{P}_2\text{O}_7)_2$ Cathode for Na-Ion Batteries. *Nano Energy* **2021**, *79*, 105417. [[CrossRef](#)]
100. Hwang, S.; Lee, Y.; Jo, E.; Chung, K.Y.; Choi, W.; Kim, S.M.; Chang, W. Investigation of Thermal Stability of $\text{P}_2\text{-Na}_x\text{CoO}_2$ Cathode Materials for Sodium Ion Batteries Using Real-Time Electron Microscopy. *ACS Appl. Mater. Interfaces* **2017**, *9*, 18883–18888. [[CrossRef](#)]
101. Feng, J.; An, Y.; Ci, L.; Xiong, S. Nonflammable Electrolyte for Safer Non-Aqueous Sodium Batteries. *J. Mater. Chem. A* **2015**, *3*, 14539–14544. [[CrossRef](#)]
102. Xie, Y.; Xu, G.-L.; Che, H.; Wang, H.; Yang, K.; Yang, X.; Guo, F.; Ren, Y.; Chen, Z.; Amine, K.; et al. Probing Thermal and Chemical Stability of $\text{Na}_x\text{Ni}_{1/3}\text{Fe}_{1/3}\text{Mn}_{1/3}\text{O}_2$ Cathode Material toward Safe Sodium-Ion Batteries. *Chem. Mater.* **2018**, *30*, 4909–4918. [[CrossRef](#)]
103. Li, Y.; Hu, Y.-S.; Qi, X.; Rong, X.; Li, H.; Huang, X.; Chen, L. Advanced Sodium-Ion Batteries Using Superior Low Cost Pyrolyzed Anthracite Anode: Towards Practical Applications. *Energy Storage Mater.* **2016**, *5*, 191–197. [[CrossRef](#)]
104. Hwang, J.-Y.; Myung, S.-T.; Choi, J.U.; Yoon, C.S.; Yashiro, H.; Sun, Y.-K. Resolving the Degradation Pathways of the O3-Type Layered Oxide Cathode Surface through the Nano-Scale Aluminum Oxide Coating for High-Energy Density Sodium-Ion Batteries. *J. Mater. Chem. A* **2017**, *5*, 23671–23680. [[CrossRef](#)]
105. Endo, K.; Zhang, H.P.; Fu, L.J.; Lee, K.J.; Sekine, K.; Takamura, T.; Jeong, Y.U.; Wu, Y.P.; Holze, R.; Wu, H.Q. Electrochemical Performance of a Novel Surface Modified Spherical Graphite as Anode Material for Lithium Ion Batteries. *J. Appl. Electrochem.* **2006**, *36*, 1307–1310. [[CrossRef](#)]
106. Shu, J. Electrochemical Behavior and Stability of $\text{Li}_4\text{Ti}_5\text{O}_12$ in a Broad Voltage Window. *J. Solid. State Electrochem.* **2009**, *13*, 1535–1539. [[CrossRef](#)]
107. Xiao, L.; Lu, H.; Fang, Y.; Sushko, M.L.; Cao, Y.; Ai, X.; Yang, H.; Liu, J. Low-Defect and Low-Porosity Hard Carbon with High Coulombic Efficiency and High Capacity for Practical Sodium Ion Battery Anode. *Adv. Energy Mater.* **2018**, *8*, 1703238. [[CrossRef](#)]

108. Yan, C.; Yuan, H.; Park, H.S.; Huang, J.-Q. Perspective on the Critical Role of Interface for Advanced Batteries. *J. Energy Chem.* **2020**, *47*, 217–220. [[CrossRef](#)]
109. Winter, M. The Solid Electrolyte Interphase—The Most Important and the Least Understood Solid Electrolyte in Rechargeable Li Batteries. *Z. Für Phys. Chem.* **2009**, *223*, 1395–1406. [[CrossRef](#)]
110. Wang, H.; Li, X.; Li, F.; Liu, X.; Yang, S.; Ma, J. Formation and Modification of Cathode Electrolyte Interphase: A Mini Review. *Electrochem. Commun.* **2021**, *122*, 106870. [[CrossRef](#)]
111. Ma, L.A.; Naylor, A.J.; Nyholm, L.; Younesi, R. Strategies for Mitigating Dissolution of Solid Electrolyte Interphases in Sodium-Ion Batteries. *Angew. Chem. Int. Ed.* **2021**, *60*, 4855–4863. [[CrossRef](#)]
112. Mogensen, R.; Brandell, D.; Younesi, R. Solubility of the Solid Electrolyte Interphase (SEI) in Sodium Ion Batteries. *ACS Energy Lett.* **2016**, *1*, 1173–1178. [[CrossRef](#)]
113. Eshetu, G.G.; Gruegeon, S.; Kim, H.; Jeong, S.; Wu, L.; Gachot, G.; Laruelle, S.; Armand, M.; Passerini, S. Comprehensive Insights into the Reactivity of Electrolytes Based on Sodium Ions. *ChemSusChem* **2016**, *9*, 462–471. [[CrossRef](#)]
114. CATL Unveils Its Latest Breakthrough Technology by Releasing Its First Generation of Sodium-Ion Batteries. Available online: <https://www.catl.com/en/news/665.html> (accessed on 23 September 2024).
115. Faradion Strong Performance. Available online: <https://faradion.co.uk/technology-benefits/strong-performance/> (accessed on 3 October 2024).
116. Rudola, A.; Wright, C.J.; Barker, J. Reviewing the Safe Shipping of Lithium-Ion and Sodium-Ion Cells: A Materials Chemistry Perspective. *Energy Mater. Adv.* **2021**, *2021*, 9798460. [[CrossRef](#)]
117. Faradion Superior Safety. Available online: <https://faradion.co.uk/technology-benefits/superior-safety/> (accessed on 23 September 2024).
118. GB/T 31845-2015; Mechanical Structures for Electrotechnical and Electronic equipment—Thermal Design Specification (English Version). Code of China: Beijing, China, 2015.
119. HiNa Achievements—Research & Development—HiNa Battery Technology Co., Ltd. Available online: <https://www.hinabattery.com/en/index.php?catid=15> (accessed on 23 September 2024).
120. CNEVPOST Hina Battery Becomes 1st Battery Maker to Put Sodium-Ion Batteries in EVs in China. Available online: <https://cnevpost.com/2023/02/23/hina-battery-puts-sodium-ion-batteries-in-sehol-e10x/> (accessed on 23 September 2024).
121. Natron Energy Battery Safety. Available online: <https://natron.energy/our-technology/safety> (accessed on 23 September 2024).
122. Natron Energy Battery Performance. Available online: <https://natron.energy/our-technology/performance> (accessed on 23 September 2024).
123. He, M.; El Mejdoubi, A.; Chartouni, D.; Morcrette, M.; Troendle, P.; Castiglioni, R. High Power NVPF/HC-Based Sodium-Ion Batteries. *J. Power Sources* **2023**, *588*, 233741. [[CrossRef](#)]
124. Bauer, A.; Song, J.; Vail, S.; Pan, W.; Barker, J.; Lu, Y. The Scale-up and Commercialization of Nonaqueous Na-Ion Battery Technologies. *Adv. Energy Mater.* **2018**, *8*, 1702869. [[CrossRef](#)]
125. Altris Altris Reaches New Milestone with 160 Wh/Kg Battery Cell. Available online: <https://www.altris.se/news/altris-reaches-new-milestone-with-160-wh-kg-battery-cell> (accessed on 23 September 2024).
126. Sodium Battery Hub Altris Sodium-Ion Batteries: Performance, Safety, and Sustainability. Available online: <https://sodiumbatteryhub.com/2024/08/02/altris-sodium-ion-batteries-performance-safety-and-sustainability/> (accessed on 23 September 2024).
127. Liaw, H.-J.; Liou, Y.-R.; Liu, P.-H.; Chen, H.-Y.; Shu, C.-M. Increased Flammability Hazard When Ionic Liquid [C₆mim][Cl] Is Exposed to High Temperatures. *J. Hazard. Mater.* **2019**, *367*, 407–417. [[CrossRef](#)]
128. 01—Home | EV Fire Safe. Available online: <https://www.evfiresafe.com/> (accessed on 22 April 2024).
129. EPRI BESS Failure Incident Database. Available online: https://storagewiki.epri.com/index.php/BESS_Failure_Incident_Database (accessed on 29 July 2024).
130. Guy, M.; Amandine, L.; Arnaud, B.; Paul, C. Truchot Benjamin Key Learnings From Recent Lithium-Ion Battery Incidents That Have Impacted e-Mobility and Energy Storage Fast Growing Markets. *Chem. Eng. Trans.* **2022**, *90*, 643–648. [[CrossRef](#)]
131. CALCE and the University of Maryland Safety. Available online: <https://web.calce.umd.edu/batteries/safety.html> (accessed on 20 September 2023).
132. Park Taejon Renault-Samsung’s Electric Vehicle Catches Fire Due to Ignition from Bonnet. Available online: <https://english.etnews.com/2016012720001> (accessed on 20 September 2023).
133. CTIF International Association of Fire and Rescue Services Large Explosion and Fire at French Lithium Battery Warehouse. Available online: <https://ctif.org/news/large-explosion-and-fire-french-lithium-battery-warehouse> (accessed on 20 September 2023).
134. South Korea: Exploding Lithium Batteries Spark Deadly Factory Fire. Available online: <https://www.bbc.com/news/articles/crgggmeyjj7o> (accessed on 9 July 2024).
135. DESTINY PhD Programme Marie Skłodowska-Curie Actions COFUND. Available online: <https://www.destiny-phd.eu/topic-22--2> (accessed on 22 April 2024).
136. Regulation—2023/1542—EN—EUR-Lex. Available online: <https://eur-lex.europa.eu/eli/reg/2023/1542/oj> (accessed on 22 April 2024).
137. Patil, A.; Patil, V.; Wook Shin, D.; Choi, J.-W.; Paik, D.-S.; Yoon, S.-J. Issue and Challenges Facing Rechargeable Thin Film Lithium Batteries. *Mater. Res. Bull.* **2008**, *43*, 1913–1942. [[CrossRef](#)]

138. Cheng, X.-B.; Zhang, R.; Zhao, C.-Z.; Wei, F.; Zhang, J.-G.; Zhang, Q. A Review of Solid Electrolyte Interphases on Lithium Metal Anode. *Adv. Sci.* **2016**, *3*, 1500213. [CrossRef]
139. An, S.J.; Li, J.; Daniel, C.; Mohanty, D.; Nagpure, S.; Wood, D.L. The State of Understanding of the Lithium-Ion-Battery Graphite Solid Electrolyte Interphase (SEI) and Its Relationship to Formation Cycling. *Carbon* **2016**, *105*, 52–76. [CrossRef]
140. Hausbrand, R. Electronic Energy Levels at Li-Ion Cathode–Liquid Electrolyte Interfaces: Concepts, Experimental Insights, and Perspectives. *J. Chem. Phys.* **2020**, *152*, 180902. [CrossRef]
141. Abe, K.; Yoshitake, H.; Kitakura, T.; Hattori, T.; Wang, H.; Yoshio, M. Additives-Containing Functional Electrolytes for Suppressing Electrolyte Decomposition in Lithium-Ion Batteries. *Electrochim. Acta* **2004**, *49*, 4613–4622. [CrossRef]
142. Cometto, C.; Yan, G.; Mariyappan, S.; Tarascon, J.-M. Means of Using Cyclic Voltammetry to Rapidly Design a Stable DMC-Based Electrolyte for Na-Ion Batteries. *J. Electrochem. Soc.* **2019**, *166*, A3723–A3730. [CrossRef]
143. Zhang, L.; Tsolakidou, C.; Mariyappan, S.; Tarascon, J.-M.; Trabesinger, S. Unraveling Gas Evolution in Sodium Batteries by Online Electrochemical Mass Spectrometry. *Energy Storage Mater.* **2021**, *42*, 12–21. [CrossRef]
144. Yan, G.; Reeves, K.; Foix, D.; Li, Z.; Cometto, C.; Mariyappan, S.; Salanne, M.; Tarascon, J. A New Electrolyte Formulation for Securing High Temperature Cycling and Storage Performances of Na-Ion Batteries. *Adv. Energy Mater.* **2019**, *9*, 1901431. [CrossRef]
145. Tran, M.-K.; Mevawalla, A.; Aziz, A.; Panchal, S.; Xie, Y.; Fowler, M. A Review of Lithium-Ion Battery Thermal Runaway Modeling and Diagnosis Approaches. *Processes* **2022**, *10*, 1192. [CrossRef]
146. Samigullin, R.R.; Drozhzhin, O.A.; Antipov, E.V. Comparative Study of the Thermal Stability of Electrode Materials for Li-Ion and Na-Ion Batteries. *ACS Appl. Energy Mater.* **2022**, *5*, 14–19. [CrossRef]
147. Julien, C.M.; Mauger, A. Fabrication of Li₄Ti₅O₁₂ (LTO) as Anode Material for Li-Ion Batteries. *Micromachines* **2024**, *15*, 310. [CrossRef]
148. Shakourian-Fard, M.; Kamath, G.; Smith, K.; Xiong, H.; Sankaranarayanan, S.K.R.S. Trends in Na-Ion Solvation with Alkyl-Carbonate Electrolytes for Sodium-Ion Batteries: Insights from First-Principles Calculations. *J. Phys. Chem. C* **2015**, *119*, 22747–22759. [CrossRef]
149. Zhou, H.; Fear, C.; Jeevarajan, J.A.; Mukherjee, P.P. State-of-Electrode (SOE) Analytics of Lithium-Ion Cells under Overdischarge Extremes. *Energy Storage Mater.* **2023**, *54*, 60–74. [CrossRef]
150. Kasnatscheew, J.; Börner, M.; Streipert, B.; Meister, P.; Wagner, R.; Cekic Laskovic, I.; Winter, M. Lithium Ion Battery Cells under Abusive Discharge Conditions: Electrode Potential Development and Interactions between Positive and Negative Electrode. *J. Power Sources* **2017**, *362*, 278–282. [CrossRef]
151. Flügel, M.; Waldmann, T.; Kasper, M.; Wohlfahrt-Mehrens, M. Detection of Copper Deposition on Anodes of Over-Discharged Lithium Ion Cells by GD-OES Depth Profiling. *ChemPhysChem* **2020**, *21*, 2047–2050. [CrossRef]
152. Rudola, A.; Rennie, A.J.R.; Heap, R.; Meysami, S.S.; Lowbridge, A.; Mazzali, F.; Sayers, R.; Wright, C.J.; Barker, J. Commercialisation of High Energy Density Sodium-Ion Batteries: Faradion’s Journey and Outlook. *J. Mater. Chem. A* **2021**, *9*, 8279–8302. [CrossRef]
153. Huo, H.; Xing, Y.; Pecht, M.; Züger, B.J.; Khare, N.; Vezzini, A. Safety Requirements for Transportation of Lithium Batteries. *Energies* **2017**, *10*, 793. [CrossRef]
154. DSV Class 9A Lithium Batteries Dangerous Goods. Available online: <https://www.dsv.com/en-gb/our-solutions/modes-of-transport/value-added-services/transporting-dangerous-goods/9-classes-of-dangerous-goods/class-9a-lithium-batteries> (accessed on 19 September 2023).
155. He, X.; Hu, Z.; Restuccia, F.; Fang, J.; Rein, G. Experimental Study of the Effect of the State of Charge on Self-Heating Ignition of Large Ensembles of Lithium-Ion Batteries in Storage. *Appl. Therm. Eng.* **2022**, *212*, 118621. [CrossRef]
156. ICAO. International Civil Aviation Organization Technical Instructions for the Safe Transport of Dangerous Goods by Air (Doc 9284) 2015–2016 Edition. Available online: <https://www.icao.int/safety/dangerousgoods/addendumcorrigendum%20to%20the%20technical%20instructions/doc%209284-2015-2016.add-3.pdf> (accessed on 3 October 2024).
157. IATA. 2024 Lithium Battery Guidance Document Transport of Lithium Metal and Lithium Ion Batteries. 2024. Available online: <https://www.iata.org/contentassets/05e6d8742b0047259bf3a700bc9d42b9/lithium-battery-guidance-document.pdf> (accessed on 3 October 2024).
158. Brennan, D. Reduced charge for vehicles powered by lithium ion, lithium metal or sodium ion batteries. In Proceedings of the Dangerous Goods Panel (DGP) Twenty-Ninth Meeting, Montréal, QC, Canada, 13 November 2023. Available online: <https://www.icao.int/safety/DangerousGoods/DGP29/DGP.29.WP.026.4.en.pdf> (accessed on 3 October 2024).
159. United Nations. *Recommendations on the Transport of Dangerous Goods Model Regulations Volume I*; United Nations: New York, NY, USA; Geneva, Switzerland, 2023.
160. UN/SCETDG/55/INF.38. Committee of Experts on the Transport of Dangerous Goods and on the Globally Harmonized System of Classification and Labelling of Chemicals. In Proceedings of the Sub-Committee of Experts on the Transport of Dangerous Goods Fifty-Fifth Session, Geneva, Switzerland, 27 June 2019.
161. Desai, P.; Huang, J.; Foix, D.; Tarascon, J.-M.; Mariyappan, S. Zero Volt Storage of Na-Ion Batteries: Performance Dependence on Cell Chemistry! *J. Power Sources* **2022**, *551*, 232177. [CrossRef]
162. Baba, Y. Thermal Stability of Li_xCoO₂ Cathode for Lithium Ion Battery. *Solid. State Ion.* **2002**, *148*, 311–316. [CrossRef]

163. MacNeil, D.D.; Dahn, J.R. The Reaction of Charged Cathodes with Nonaqueous Solvents and Electrolytes: I. $\text{Li}_{0.5}\text{CoO}_2$. *J. Electrochem. Soc.* **2001**, *148*, A1205. [[CrossRef](#)]
164. MacNeil, D.D.; Dahn, J.R. The Reactions of $\text{Li}[\text{Sub } 0.5]\text{CoO}[\text{Sub } 2]$ with Nonaqueous Solvents at Elevated Temperatures. *J. Electrochem. Soc.* **2002**, *149*, A912. [[CrossRef](#)]
165. Hossain, M.S.; Furusawa, T.; Sato, M. Hydrothermal Synthesis, Characterization and Thermal Stability Studies of $\alpha\text{-Fe}_2\text{O}_3$ Hollow Microspheres. *Adv. Powder Technol.* **2022**, *33*, 103797. [[CrossRef](#)]
166. Darezereshki, E.; Bakhtiari, F.; Alizadeh, M.; Behrad Vakylabad, A.; Ranjbar, M. Direct Thermal Decomposition Synthesis and Characterization of Hematite ($\alpha\text{-Fe}_2\text{O}_3$) Nanoparticles. *Mater. Sci. Semicond. Process.* **2012**, *15*, 91–97. [[CrossRef](#)]
167. Yang, H.; Zhang, Q.; Chen, M.; Yang, Y.; Zhao, J. Unveiling the Origin of Air Stability in Polyanion and Layered-Oxide Cathode Materials for Sodium-Ion Batteries and Their Practical Application Considerations. *Adv. Funct. Mater.* **2024**, *34*, 2308257. [[CrossRef](#)]
168. Zhao, J.; Zhao, L.; Chihara, K.; Okada, S.; Yamaki, J.; Matsumoto, S.; Kuze, S.; Nakane, K. Electrochemical and Thermal Properties of Hard Carbon-Type Anodes for Na-Ion Batteries. *J. Power Sources* **2013**, *244*, 752–757. [[CrossRef](#)]
169. SODIUM PERCHLORATE | CAMEO Chemicals | NOAA. Available online: <https://cameochemicals.noaa.gov/chemical/1514> (accessed on 26 April 2024).
170. Bhutia, P.T.; Grugeon, S.; Bertrand, J.-P.; Binotto, G.; Bordes, A.; El Mejdoubi, A.; Laruelle, S.; Marlair, G. Fire Hazards of Carbonate-Based Electrolytes for Sodium-Ion Batteries: What Changes from Lithium-Ion Batteries? *J. Power Sources* **2024**, *622*, 235234. [[CrossRef](#)]
171. Tribouilloy Benoit; Paillery Esteban; Binotto Ghislain; Marlair Guy Flammability of Halogenated Liquids: Flash Points Limits. *Chem. Eng. Trans.* **2022**, *90*, 529–534. [[CrossRef](#)]
172. Yang, Z.; He, J.; Lai, W.; Peng, J.; Liu, X.; He, X.; Guo, X.; Li, L.; Qiao, Y.; Ma, J.; et al. Fire-Retardant, Stable-Cycling and High-Safety Sodium Ion Battery. *Angew. Chem.* **2021**, *133*, 27292–27300. [[CrossRef](#)]
173. Velencoso, M.M.; Battig, A.; Markwart, J.C.; Schartel, B.; Wurm, F.R. Molecular Firefighting—How Modern Phosphorus Chemistry Can Help Solve the Challenge of Flame Retardancy. *Angew. Chem. Int. Ed.* **2018**, *57*, 10450–10467. [[CrossRef](#)]
174. Xu, X.; Lin, K.; Zhou, D.; Liu, Q.; Qin, X.; Wang, S.; He, S.; Kang, F.; Li, B.; Wang, G. Quasi-Solid-State Dual-Ion Sodium Metal Batteries for Low-Cost Energy Storage. *Chem.* **2020**, *6*, 902–918. [[CrossRef](#)]
175. Zhou, Q.; Dong, S.; Lv, Z.; Xu, G.; Huang, L.; Wang, Q.; Cui, Z.; Cui, G. A Temperature-Responsive Electrolyte Endowing Superior Safety Characteristic of Lithium Metal Batteries. *Adv. Energy Mater.* **2020**, *10*, 1903441. [[CrossRef](#)]
176. Kumar, D.; Yadav, N.; Mishra, K.; Shahid, R.; Arif, T.; Kanchan, D.K. Sodium Ion Conducting Flame-Retardant Gel Polymer Electrolyte for Sodium Batteries and Electric Double Layer Capacitors (EDLCs). *J. Energy Storage* **2022**, *46*, 103899. [[CrossRef](#)]
177. Yang, H.; Tian, W.; Chen, X.; Li, Z.; Liu, P.; Wang, Q.; Nie, X.; Wang, Q.; Jiao, L. Flame-Retardant Polymer Electrolyte for Sodium-Ion Batteries. *Batter. Supercaps* **2024**, *e202400383*. [[CrossRef](#)]
178. Hyung, Y.E.; Vissers, D.R.; Amine, K. Flame-Retardant Additives for Lithium-Ion Batteries. *J. Power Sources* **2003**, *119–121*, 383–387. [[CrossRef](#)]
179. Lee, C.W. A Novel Flame-Retardant Additive for Lithium Batteries. *Electrochim. Solid-State Lett.* **1999**, *3*, 63. [[CrossRef](#)]
180. Belov, D.G.; Shieh, D.T. A Study of Tetrabromobisphenol A (TBBA) as a Flame Retardant Additive for Li-Ion Battery Electrolytes. *J. Power Sources* **2014**, *247*, 865–875. [[CrossRef](#)]
181. Bordes, A.; Marlair, G.; Zantman, A.; Chesnaye, A.; Lore, P.-A.L.; Lecocq, A. Safety Evaluation of a Sodium-Ion Cell: Assessment of Vent Gas Emissions under Thermal Runaway. *ACS Energy Lett.* **2022**, *7*, 3386–3391. [[CrossRef](#)]
182. Bordes, A.; Marlair, G.; Zantman, A.; Herreyre, S.; Papin, A.; Desprez, P.; Lecocq, A. New Insight on the Risk Profile Pertaining to Lithium-Ion Batteries under Thermal Runaway as Affected by System Modularity and Subsequent Oxidation Regime. *J. Energy Storage* **2022**, *52*, 104790. [[CrossRef](#)]
183. Fernandes, Y.; Bry, A.; De Persis, S. Identification and Quantification of Gases Emitted during Abuse Tests by Overcharge of a Commercial Li-Ion Battery. *J. Power Sources* **2018**, *389*, 106–119. [[CrossRef](#)]
184. Yang, X.; Wang, H.; Li, M.; Li, Y.; Li, C.; Zhang, Y.; Chen, S.; Shen, H.; Qian, F.; Feng, X.; et al. Experimental Study on Thermal Runaway Behavior of Lithium-Ion Battery and Analysis of Combustible Limit of Gas Production. *Batteries* **2022**, *8*, 250. [[CrossRef](#)]
185. Bugryniec, P.J.; Davidson, J.N.; Brown, S.F. Assessment of Thermal Runaway in Commercial Lithium Iron Phosphate Cells Due to Overheating in an Oven Test. *Energy Procedia* **2018**, *151*, 74–78. [[CrossRef](#)]
186. Townsend, D.I.; Tou, J.C. Thermal Hazard Evaluation by an Accelerating Rate Calorimeter. *Thermochim. Acta* **1980**, *37*, 1–30. [[CrossRef](#)]
187. Jhu, C.-Y.; Wang, Y.-W.; Wen, C.-Y.; Shu, C.-M. Thermal Runaway Potential of LiCoO_2 and $\text{Li}(\text{Ni}_{1/3}\text{Co}_{1/3}\text{Mn}_{1/3})\text{O}_2$ Batteries Determined with Adiabatic Calorimetry Methodology. *Appl. Energy* **2012**, *100*, 127–131. [[CrossRef](#)]
188. Lei, B.; Zhao, W.; Ziebert, C.; Uhlmann, N.; Rohde, M.; Seifert, H. Experimental Analysis of Thermal Runaway in 18650 Cylindrical Li-Ion Cells Using an Accelerating Rate Calorimeter. *Batteries* **2017**, *3*, 14. [[CrossRef](#)]
189. Rosalind, E. Franklin Crystallite Growth in Graphitizing and Non-Graphitizing Carbons. *Proc. R. Soc. Lond. A* **1951**, *209*, 196–218. [[CrossRef](#)]
190. Ren, J.; Zhu, H.; Fang, Y.; Li, W.; Lan, S.; Wei, S.; Yin, Z.; Tang, Y.; Ren, Y.; Liu, Q. Typical Cathode Materials for Lithium-ion and Sodium-ion Batteries: From Structural Design to Performance Optimization. *Carbon. Neutralization* **2023**, *2*, 339–377. [[CrossRef](#)]

191. Darga, J.; Lamb, J.; Manthiram, A. Industrialization of Layered Oxide Cathodes for Lithium-Ion and Sodium-Ion Batteries: A Comparative Perspective. *Energy Tech.* **2020**, *8*, 2000723. [[CrossRef](#)]
192. Pan, Y.; Chou, S.; Liu, H.K.; Dou, S.X. Functional Membrane Separators for Next-Generation High-Energy Rechargeable Batteries. *Natl. Sci. Rev.* **2017**, *4*, 917–933. [[CrossRef](#)]
193. Arora, P.; Zhang, Z. (John) Battery Separators. *Chem. Rev.* **2004**, *104*, 4419–4462. [[CrossRef](#)]
194. Li, A.; Yuen, A.C.Y.; Wang, W.; De Cachinho Cordeiro, I.M.; Wang, C.; Chen, T.B.Y.; Zhang, J.; Chan, Q.N.; Yeoh, G.H. A Review on Lithium-Ion Battery Separators towards Enhanced Safety Performances and Modelling Approaches. *Molecules* **2021**, *26*, 478. [[CrossRef](#)]
195. Orendorff, C.J. The Role of Separators in Lithium-Ion Cell Safety. *Interface Mag.* **2012**, *21*, 61–65. [[CrossRef](#)]
196. Zhou, H.; Fear, C.; Parekh, M.; Gray, F.; Fleetwood, J.; Adams, T.; Tomar, V.; Pol, V.G.; Mukherjee, P.P. The Role of Separator Thermal Stability in Safety Characteristics of Lithium-Ion Batteries. *J. Electrochem. Soc.* **2022**, *169*, 090521. [[CrossRef](#)]
197. Deimede, V.; Elmasides, C. Separators for Lithium-Ion Batteries: A Review on the Production Processes and Recent Developments. *Energy Technol.* **2015**, *3*, 453–468. [[CrossRef](#)]
198. Zu, C.; Li, J.; Cai, B.; Qiu, J.; Zhao, Y.; Yang, Q.; Li, H.; Yu, H. Separators with Reactive Metal Oxide Coatings for Dendrite-Free Lithium Metal Anodes. *J. Power Sources* **2023**, *555*, 232336. [[CrossRef](#)]
199. Ho, V.; Nguyen, B.T.D.; Thi, H.Y.N.; Kim, J.F.; Mun, J. Poly(Dopamine) Surface-modified Polyethylene Separator with Electrolytephilic Characteristics for Enhancing the Performance of Sodium-ion Batteries. *Intl J. Energy Res.* **2022**, *46*, 5177–5188. [[CrossRef](#)]
200. Kim, J.I.; Heo, J.; Park, J.H. Tailored Metal Oxide Thin Film on Polyethylene Separators for Sodium-Ion Batteries. *J. Electrochem. Soc.* **2017**, *164*, A1965–A1969. [[CrossRef](#)]

Disclaimer/Publisher's Note: The statements, opinions and data contained in all publications are solely those of the individual author(s) and contributor(s) and not of MDPI and/or the editor(s). MDPI and/or the editor(s) disclaim responsibility for any injury to people or property resulting from any ideas, methods, instructions or products referred to in the content.